Spontaneous emergence and drifting of sequential neural activity in recurrent networks

Shuai Shao[1,2,3], Juan Luis Riquelme[1,*], Julijana Gjorgjieva[3,*]

1 Max Planck Institute for Brain Research, Frankfurt, Germany
2 Donders Institute and Faculty of Science, Radboud University, Nijmegen, Netherlands
3 School of Life Sciences, Technical University of Munich, Freising, Germany
*Correspondence: gjorgjieva@tum.de; juan.riquelme@brain.mpg.de

Abstract

Repeating sequences of neural activity exist across diverse brain regions of different animals and are thought to underlie diverse computations. However, their emergence and evolution in the presence of ongoing synaptic plasticity remain poorly understood. To gain mechanistic insights into this process, we modeled how biologically-inspired rules of activity-dependent synaptic plasticity in recurrent circuits interact to produce connectivity structures that support sequential neuronal activity. Even under unstructured inputs, our recurrent networks developed strong unidirectional connections, resulting in spontaneous repeating spiking sequences. During ongoing plasticity these sequences repeated despite turnover of individual synaptic connections, a process reminiscent of synaptic drift. The turnover process occurred over different timescales, with certain connectivity types and motif structures leading to sequences with different volatility. Structured inputs could reinforce or retrain the resulting connectivity structures underlying sequences, enabling stable but still flexible encoding of inputs. Our model unveils the interplay between synaptic plasticity and sequential activity in recurrent networks, providing insights into how brains implement reliable but flexible computations.

Introduction

Repeating sequences of neural activity are reported across many species and brain regions, including in the navigational, sensory, and motor areas of mammals, reptiles, and birds, and believed to underlie many computations. Perhaps the most striking example of repeating sequences is in the motor area of songbirds [1]. Zebrafinches repeat their courtship song thousands of times with a perfectly matching sequential representation in their brain. In the hippocampus of rats, sequences of spikes encode place trajectories as the animal moves, and they are replayed during rest [2, 3]. Repeating sequences of spikes are also common in the sensory cortices of rats, humans, mice, and turtles [4–7]. Yet, whether and how these sequences emerge and change over time to flexibly implement these computations remains poorly understood.

However, the reported sequences are hardly stereotyped. An increasing body of experimental evidence shows that representations in multiple brain areas are often subject to “drift” [8–12] where one neuronal

pattern of activations is slowly replaced by another. In the hippocampus, after the mapping of space is established [13–15], after the animals have been trained in the same environment and place fields have formed, spontaneous changes in the encoding, a phenomenon known as "remapping", reorganize the existing sequences [16, 17]. In the birdsong system, sequences are first learned and heavily modified by the juvenile bird as it develops its own version before the song crystallizes [18]. Even as an adult, the song can be modified under acute manipulations of their auditory system, indicative of the ongoing plasticity to which it is exposed [19, 20]. These sequences of spikes are not fixed ensembles as observed in partial out-of-order reproductions during sleep [21]. Even though the zebra finch is a specialist of one song, it still produces other non-courtship vocalizations in adulthood using the same motor areas [22–24]. Related species such as budgerigars, bengalese finches and canaries present more variable songs and even life-long learning, suggesting that the neuronal substrate underlying the sequences may be more plastic than typically assumed [25–27].

The specific processes driving these fast and slow changes in sequences of neural activations are unknown, but likely relate to activity-dependent synaptic plasticity due to sensory experience [28, 29] or developmental spontaneous activity prior to the onset of sensory experience [30, 31]. Indeed, a plethora of plasticity mechanisms have been studied, theoretically and experimentally, and are considered the main actors of organization of recurrent networks of neurons [32–37]. Experimental and theoretical evidence has put forward spike-timing-dependent plasticity (STDP) as the underlying plasticity mechanism which describes synaptic change based on the order and timing of pre- and postsynaptic spikes [33, 34, 38]. Nonetheless, many forms of STDP have been described, which depend on pairs or triplets of spikes, operate at different timescales and have Hebbian or anti-Hebbian effects, depending on which order of the spikes induces potentiation or depression [33, 35, 39–41]. Moreover, these STDP rules depend on brain region, cell type, and the presence of different neuromodulators [42, 43]. These different forms of STDP can have different influences on recurrent network connectivity. For example, Hebbian forms of symmetric pair-based STDP, shifted asymmetric STDP, or rate-dependent triplet STDP has been shown to promote the formation of "neuronal assemblies" [40, 41, 44–46], groups of neurons sharing strong connections and exhibiting coordinated firing [44, 47]. In contrast, anti-symmetric Hebbian STDP has been shown to promote the formation of "synfire chains", a form of idealized sequential structures [35]. What specific synaptic plasticity rules promote structures of directed connectivity characteristic of the repeatable, but still flexible sequential activity widely seen experimentally, is still unknown. Furthermore, if plasticity, structure and activity are interlocked in a recurrent loop where each one drives the next, one might assume that repeating neuronal patterns might be self-preserving and a fixed phenomenon. Previous theoretical work has suggested that sequences provide stable output and robustly encode memories despite ongoing plastic processes [48, 49]. However, if, as described above, neuronal representations are subject to constant change, driven through either internal dynamics or external stimuli, we lack an understanding of how this change affects the repeatability of sequences and their underlying structures.

How repeatable are sequences of neuronal activations that occur in an intrinsically plastic system such as cortex? Here, we asked how activity-dependent synaptic plasticity may naturally produce the connectivity structures underlying repeatable sequences, and how these very same plasticity mechanisms alter them. To mechanistically dissect this question, we built a recurrent, plastic, spiking network model that produced sequences that repeated but also evolved. Driven by unstructured activity, the network spontaneously developed connectivity structures that led to the appearance of spiking sequences. However, these same plastic processes also created volatile dynamics of synaptic turnover with different timescales

depending on synapse type, strength and connectivity motifs. Exposing the network to structured inputs revealed that the same plasticity mechanisms under random dynamics could stabilize patterns over extended periods, remaining flexible to re-encode new inputs. Overall, our work addresses how the interaction between plasticity rules and mechanisms of sequential propagation lead to stability and adaptability in neural networks, which is crucial to understand neuronal representations and learning in dynamic environments.

Results

Synaptic strengths generated by plasticity produce repeating sequences

Long-tailed distributions of synaptic strengths can be sufficient for generating reliable sequential neural activity [50]. Thus, we first focused on identifying plasticity rules that produced such distributions in random networks and verified that they produced sequential activity. We built a neural network with randomly connected excitatory (E) and inhibitory (I) adaptive exponential integrate-and-fire neurons [51] (Fig. 1A). We modeled spontaneous activity as uncorrelated Poisson inputs independently sampled for every neuron. E-to-E and I-to-E connections followed spike-timing-dependent plasticity rules (eSTDP and iSTDP respectively, Fig. 1A) [34, 38, 52] and were subject to weight normalization [53, 54]). In addition, excitatory neurons experienced intrinsic synaptic plasticity [55, 56] which adjusted their firing thresholds to their firing rate, preventing any small fraction of the neurons from dominating the entire network.

Since intrinsic plasticity adjusted the firing thresholds, we studied synaptic strengths after scaling them by the distance between the post-synaptic neuron's threshold and resting potentials. We refer to this value as *effective* weight ($W_{\text{eff}} = W/(V_{th} - V_0)$), which provides a good indicator of the likelihood that a presynaptic activation would trigger a postsynaptic spike (Fig. 1B). The steady state of the plastic network subjected to uncorrelated inputs resulted in an E-to-E effective weight distribution that was skewed, with a long tail well described by a lognormal distribution (Fig. 1C). We found that the rare strong connections in the tail of the distribution were distributed among the whole excitatory population, with most excitatory neurons having at least one such connection (Fig. 1D).

To test the generation of sequences, we randomly selected an excitatory neuron (source neuron) in the model network, forced it to produce spikes at regular intervals (Fig. 1E) and measured the response of all other neurons in the network. Plasticity was turned off only during this testing in our simulations. Each of the 1,000 source spikes defined a trial. We quantified the resulting firing rate modulation as the difference between each neuron's firing rate after and before the source neuron spikes. We call "followers" those neurons that exhibited a significantly high firing rate modulation when compared to a null model with no injected spikes (Methods). Out of 155 tested source neurons in a model network, 135 (87.1%) of them had at least one excitatory follower (Fig. S1). The median number of excitatory followers (excluding 0) was 55, and source neurons could have more than 120 excitatory followers (Fig. S1A).

Source spikes caused the activation of followers in the same sequence across trials (Fig. 1E, S2, and S3, [7]). Followers could activate after the source spike with a delay up to 150 ms, much longer than the timescales of neuronal dynamics. Different subsets of all followers fired in every single trial (55% excitatory and 74% inhibitory followers per trial on average, S1B). We thus defined the responding probability of a follower as the ratio out of all trials in which it fired at least once within 300 ms from the source spike. Across all followers, the median delay and the jitter increased together, while both of them decreased with increasing responding probability (Fig. 1F, Fig. S4).

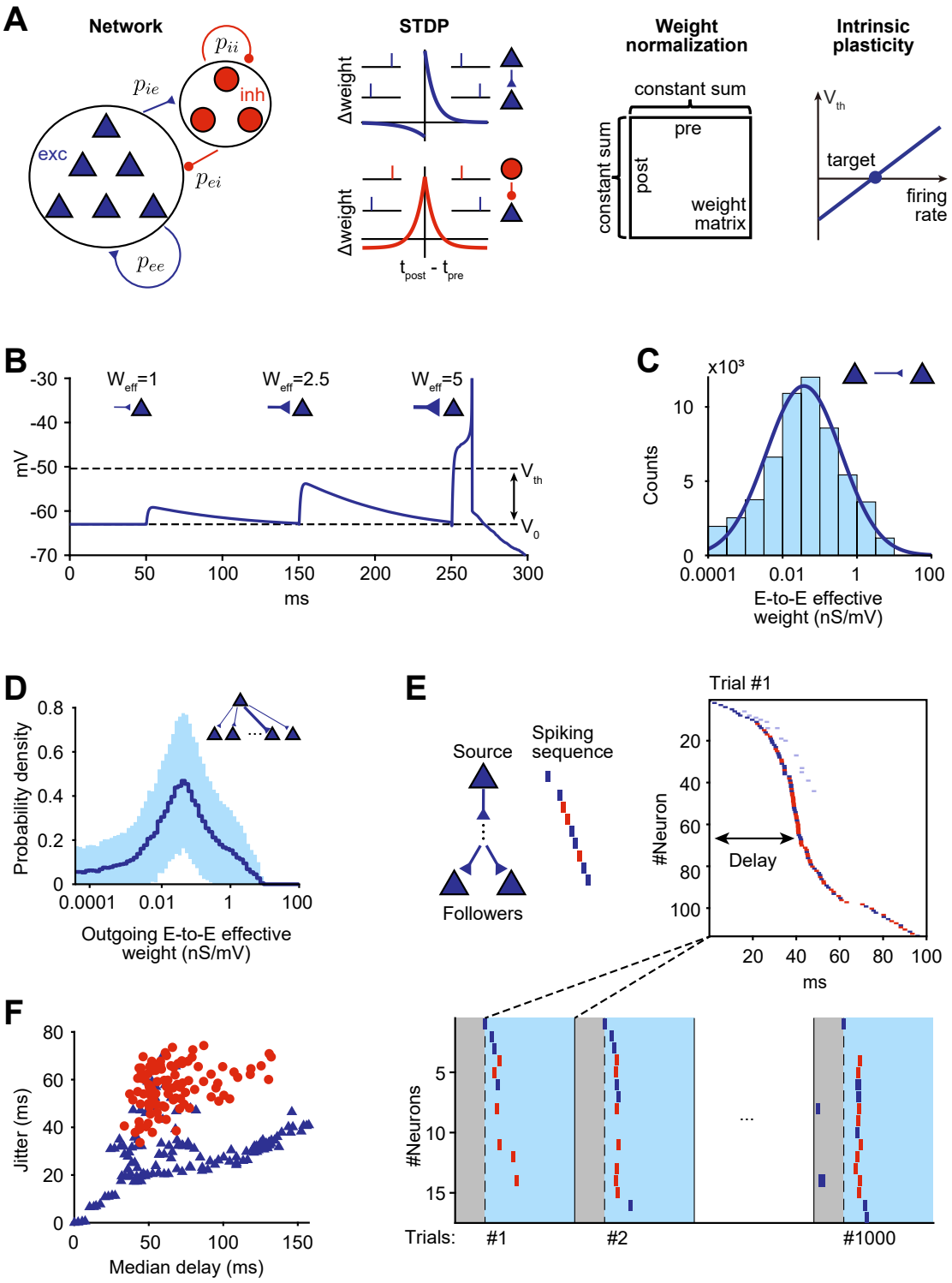

Figure 1. (Caption on the next page.)

Surprisingly, although the model lacked E-to-I plasticity and thus could not produce strong connections onto inhibitory neurons, it did produce inhibitory followers (median: 33, 45.8% of source neurons) (Fig. S1).

Figure 1. A plastic recurrent network can generate sequences under unstructured inputs. A. Schematic of the model network with 1,200 excitatory and 240 inhibitory AdEx neurons, where E-to-E connections follow a Hebbian pair-based eSTDP rule and I-to-E connections follow a pair-based iSTDP rule. Synaptic normalization preserves the total sum of incoming and outgoing weights (E-to-E and I-to-E). Intrinsic adjusts the firing threshold of excitatory neurons if the firing rate is higher or lower than the target firing rate. **B.** Example EPSPs initiated by connections with different W_{eff} on an isolated neuron. The effective weight of a connection (W_{eff}) depends on the synaptic weight (W), the postsynaptic resting potential (V_0), and the firing threshold (V_{th}). **C.** The network develops a lognormal E-to-E weight distribution in the steady-state. **D.** Different presynaptic neurons have similarly-distributed output connections. Solid line indicates the average and shade represents the standard deviation. Pooled over all E neurons in the network ($n = 1,200$). **E.** Top: When a randomly chosen "source" neuron is forced to spike, its "followers" activate reliably and sequentially. Neurons are sorted by their spike time in example trial. Blue and red ticks indicate excitatory and inhibitory followers. Bottom: the source neuron was forced to spike in 1,000 consecutive trials and increases in firing rate were calculated to identify reliable followers. **F.** The jitter of the followers is positively correlated with the median delay. Same followers as E.

Compared to excitatory followers with the same responding probability or median delay, inhibitory followers had a larger jitter (Fig. 1F and S3). We found that the activation of inhibitory followers results in feedback inhibition onto the source neuron (Fig. S5), possibly explaining post-spike hyperpolarization observed experimentally [7].

In summary, plasticity in our network generated connectivity that promotes the appearance of sequences even under random inputs. Single spikes in most excitatory neurons reliably trigger sequences of spikes in the rest of the network that repeat from trial to trial.

Strong excitatory connections resist turnover under uncorrelated inputs

Although our model network converged to a steady state in terms of the distribution of effective weights, individual connections were still under the effects of ongoing plasticity (distribution and single example connections tracked in Fig. 2A). Since sequences in our networks are mainly driven by strong connections [50], these changes could limit the capacity of the network to produce repeatable sequences over long timescales.

We first defined the ratio of strong E-to-E connections to the number of all possible E-to-E connections ($p_{ee}N_e(N_e-1)$, Fig. 2B). Once the steady state was reached, our network could always produce sequences as a consequence of a stable number of strong connections distributed over the network independent of their exact identity. When we tracked small groups of E-to-E connections that lived in the tail of the distribution at a given time point ($W_{\text{eff}} > 2.5$, Fig. S1D), we found that they had been weak in the past and would become weak again in the future (Fig. 2C). This group would then be replaced by a new group of connections preserving the tail of the distribution. Strong I-to-E connections followed the same dynamics (Fig. S6A). Indeed, under our uncorrelated inputs, the probability that a connection remained strong after a given period decayed exponentially (Fig. 2D, blue).

Is the decay of strong connections slow or fast compared to network dynamics? To establish a decay baseline, we simulated a baseline network, under the same plasticity rules, where all the neurons generated independent Poisson spikes with the same rate as our network simulations (Fig. 2D, gray). We found the decay of strong connections was much slower than this random baseline. This slowed decay is likely the product of the synaptic potentiation resulting from the anti-symmetric eSTDP rule combined with

positive spiking correlations between pre and post synaptic units. Indeed, I-to-E connections, subject to symmetric iSTDP and negative correlations resulting from inhibition, showed decays very close to baseline (Fig. 2D, red).

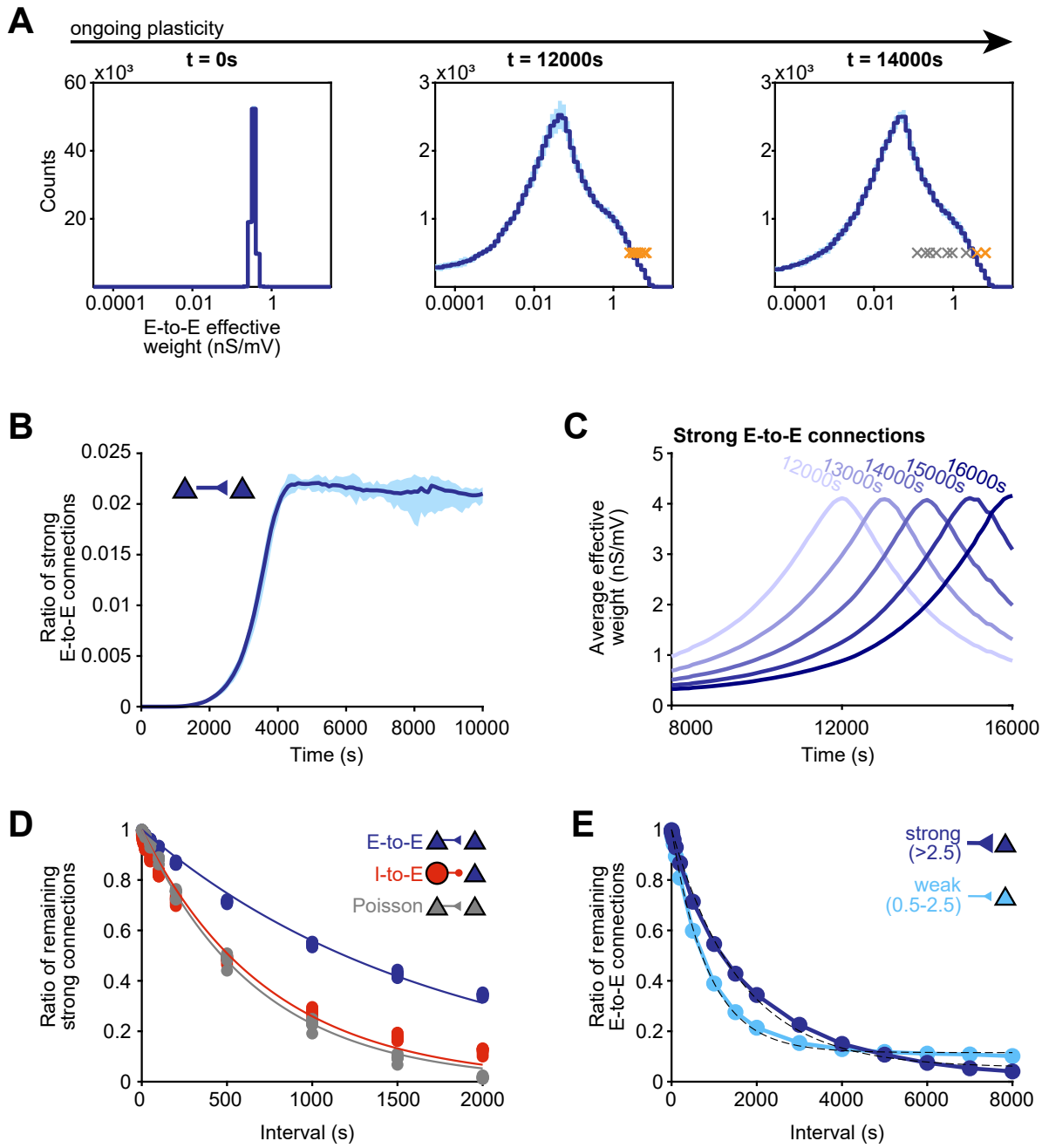

Figure 2. (Caption on the next page.)

Strong E-to-E connections were not just slower in decay when compared to I-to-E, but also when compared to weak E-to-E connections in the body of the distribution. We quantified the turnover of weak connections ($W_{\text{eff}} \in (0.5, 2.5]$) as the ratio of connections that remained above their lower bound after some

Figure 2. Turnover of strong connections in the plastic network. A. Evolution of weight distribution (line and shading; mean±std) and example single connections (crosses) at multiple time points. Colored crosses indicate strong connections ($W_{\text{eff}} > 2.5$). The distribution reaches a steady state, but single connections continue to fluctuate in strength. **B.** Ratio of strong E-to-E connections over time. **C.** Average strength of multiple groups of E-to-E connections randomly picked from the tail of the distribution at different time points (colored labels), after the weight distribution has reached a steady state. **D.** Decay rate of strong E-to-E (blue) and I-to-E connections (red). Dots indicate the ratio of strong connections that remain strong after a given interval (abscissa). Lines indicate exponential fits. Gray represents E-to-E connections when neurons are forced to fire Poisson spike trains. $\tau_{ee} = 1,719$ s, $\tau_{ie} = 741$ s, $\tau_{poisson} = 679$ s, $n = 10$ networks. **E.** Decay rate of strong E-to-E ($W_{\text{eff}} > 2.5$, same as the average of blue points in **D**, up to 2,000 s) and weak E-to-E connections ($0.5 < W_{\text{eff}} \leq 2.5$, $n = 10$ networks). Dashed lines indicate exponential fits with baseline.

elapsed time. The ratio first decreased and then saturated (Fig. 2E and S6B), and could be described with an exponential function and a baseline, i.e., $1 - a\,[1 - \exp(-t/\tau)]$. The time constant for weak connections ($\tau = 856$ s) was of the same scale as our baseline and I-to-E fit (Fig. 2D, gray and red) and again much shorter than that of strong connections ($W_{\text{eff}} > 2.5$; $\tau = 1,605$ s). Interestingly, I-to-E connections showed the opposite trend: strong connections decayed slightly faster ($W_{\text{eff}} > 2.5$; $\tau = 599$ s) than weak ones ($W_{\text{eff}} \in (0.5, 2.5]$; $\tau = 781$ s) (Fig. S6B).

In summary, under uncorrelated inputs and ongoing plasticity, our networks displayed stability at the global level of synaptic strength distributions, but volatility of individual connections. While all connections experienced turnover in their strength, the strongest E-to-E connections displayed slower decay than the rest of the network. These strong connections thus provide a backbone of sequential activity.

Plasticity promotes connectivity motifs involved in sequential propagation

While single strong connections are key to sequences of spikes in our networks, studies have shown that certain connectivity motifs are more likely to appear or to be activated in recurrent cortical networks [50, 57–60]. Hence, we next investigated how plasticity structures the connectivity motifs of our networks and their role in the propagation of sequential activity.

We focused on four 3-neuron motif types composed of strong E-to-E connections: linear chains, divergence motifs, convergence motifs and fan-in/out motifs ($W_{\text{eff}} > 2.5$, Fig. 3A). Note that one more 3-neuron motif is possible: a cycle motif, where all three neurons are connected in a recurrent loop [59, 61]. However, due to the asymmetry of the eSTDP rule, the cycle motif was extremely unlikely in our network (similar to [61]), with an average of 0.08 motifs per network instance.

We defined the ratio of number of detected motifs divided by the total number of possible sites to form a motif (see Methods for each motif). When we tracked the ratio of each motif type, we observed a sudden increase in the ratio of strong motifs for all motif types, followed by a steady state (Fig. 3B). This increase mimicked that observed for single connections (Fig. 2B), but was not merely a consequence of it. When we estimated the ratio of motifs in a random network, given the same probability of strong unidirectional connections, we found that our steady-state networks over-represented "fan-in/out" motifs and under-represented all other motif types (Fig. 3C).

We hypothesized that the presence of convergence and divergence motifs was limited by the competition between multiple connections on a single neuron that results from weight normalization. Additionally, intrinsic plasticity, by imposing the same target firing rate on all neurons, also discourages the clustering

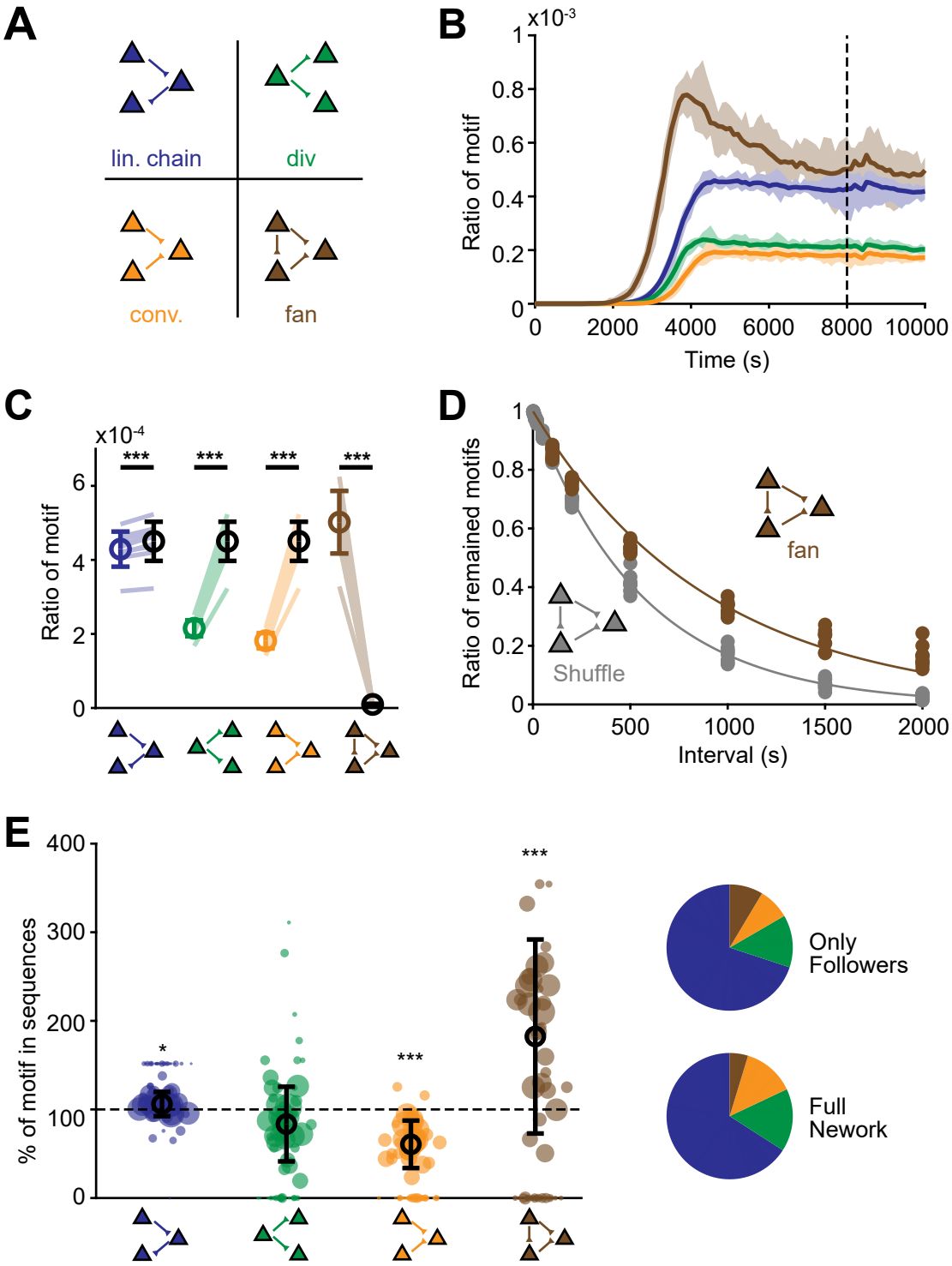

Figure 3. (Caption on the next page.)

of strong connections on single neurons required for these motifs. To verify this hypothesis, we disabled the presynaptic weight normalization and intrinsic plasticity on E neurons in new simulations. We found all of the motif ratios in these alternative models were above random levels (Fig. S7A), but the ratio of

Figure 3. Motif analysis of strong connections. A. Definitions of the four triplet motifs: linear chains, divergence motifs, convergence motifs, and fan-in/out motifs. **B.** Ratio of triplet motifs of strong connections over time, relative to the number of all possible sites to form a motif. The dashed line corresponds to the data points in **C**. **C.** Ratio of motifs in our model network and the estimated ratio in a random network with the same ratio of strong E-to-E connections ($n = 10$ networks; mean$\pm$std). ***: $P < 0.001$, paired sample t-test. **D.** Decay rate of the fan-in/out motif (colored) compared to a null model (gray) with shuffled connections. Lines indicate exponential fits ($\tau_{fan} = 907$ s $\tau_{shuffle} = 562$ s). **E.** Percentage of motifs among followers relative to the percentage among all neurons in the network ($n = 74$ sequences; mean $\pm$ std). Pie charts: percentages among followers (linear chains: 69.95%; divergence: 13.42%; convergence: 8.05%; fan-in/out: 8.58%, summing up to 100%) and in the full network (linear chains: 65.94%; divergence: 16.08%; convergence: 13.28%; fan-in/out: 4.70%, summing up to 100%). *: $P < 0.05$, ***: $P < 0.001$, single sample t-test.

strong connections was lower (2.1×10^{-3} vs. 0.021). This alternative model contained a small number (4%) of neurons that receive from or give away to other neurons most of the strong connections. These "hub" neurons also fired much more frequently than average, exerting a large impact on the network dynamics (Fig. S7B, [62–64]). Only $\sim$5% of the excitatory neurons (the hub neurons) had followers and their activation was very short lived ($<$20ms), closer to synchronous firing than to sequential propagation (Fig. S7C-D). We concluded that the plasticity rules that promote the homogeneous distribution of strong connections required for sequential activity simultaneously limit the presence of divergent and convergent motifs. If this argument were true, then fan-in/out motifs should also be limited by the plastic mechanisms described above. Removing any one of the three strong connections from a fan-in/out motif transforms it into one of the other three studied here. Given the turnover of single strong connections (Fig. 2B), it is thus surprising that fan-in/out motifs were so over-represented.

An alternative hypothesis for the over-representation of fan-in/out motifs is self-reinforcement. To test this, we explored the turnover rate of the fan-in/out motif relative to single strong connections. We thus established a baseline where we exchanged a random selection of strong connections with weak ones to achieve the same turnover rate of individual strong E-to-E connections as before (Fig. 2D). The decay time constant of the shuffled fan-in/out motifs was approximately 1/3 of the time constant of strong unidirectional connections under normal turnover (i.e., $\tau'_{\text{motif}} \simeq \tau_{\text{ee}}/3$) (Fig. 2D). In contrast, fan-in/out motifs decayed more slowly than this baseline (Fig. 3D). Therefore, the slow decay of the fan-in/out motif could not be ascribed exclusively to the slow decay of single strong connections, but rather indicates the existence of higher-order self-reinforcing effects, likely driven through the effect of eSTDP. When we performed equivalent analysis for the other motif types, we observed faster-than-expected decays (Fig. S8), showing that these motifs are not only less common but also highly volatile.

We then evaluated if these motifs supported sequential propagation specifically. We considered only the E-to-E connections among the source neuron and its most reliable followers (responding probability $\geq$ 0.8). We calculated the relative percentage of each motif type (Fig. 3E, top pie chart), then normalized the motif percentages in the sequences by the motif percentages for the full network (Fig. 3E, bottom pie chart). We found that the fan-in/out motifs appeared even more frequently among followers than in the full network, where they are already over-represented (Fig. 3E, dots).

Taken together, our results show that plasticity rules produce specific structures of connectivity that support the reliable propagation of sequential activity. Fan-in/out motifs of strong connections self-reinforce, resulting in a slow decay of the motif and their over-representation across the entire network and among

followers. Convergence and divergence motifs on the other hand are suppressed through heterosynaptic plasticity, which promotes an homogeneous distribution of strong connections within the network.

Turnover of strong connections causes a turnover in sequence composition

The decay of strong E-to-E connections and fan-in/out motifs, despite being slower than other network dynamics, can cause their disappearance and therefore the destruction of sequential structure. However, network statistics, such as the distribution of synaptic strengths, remain stable, suggesting that new sequences emerge. Indeed, sequences initiated by the same source neuron at different time points exhibited different follower compositions, where some remained, some were lost, and new ones appeared (Fig. 4A). We compared new and lost followers within 100 s intervals and averaged over 50 sequences (Fig. 4B). The net increase of the number of followers (new - lost) in a 100 s interval was -0.1 ± 30.6, indicating that the size of the sequences remained stable over time.

To evaluate the speed of follower turnover, we first pooled 2,931 followers from 50 randomly selected source neurons over 10 model networks trained with the same plasticity rules and parameters. The followers were detected at the steady state of the network ($t = 8,000$ s). We then re-evaluated if these neurons continued to classify as followers at regular intervals within the steady state. We found that the ratio of initial followers that remain followers dropped exponentially (Fig. 4C).

The time constant of follower turnover was much shorter than that of strong connections (Fig. 2D). To characterize the differences in turnover rates among followers, we analyzed followers based on their responding probabilities and delays. We found that the ratio of remaining followers was the highest for followers with the highest responding probability and shortest delay (Fig. 4D, Fig. S9A). Considering that strong E-to-E connections are the main conduit of follower activation (Fig. 1, [50]), we calculated the length of the shortest path connecting each follower to its source using only strong E-to-E connections (which we call “synaptic jumps”). The length of this path negatively correlated with the follower’s responding probability and positively correlated with its median delay (Fig. S9B-C). Consistent with these correlations, the remaining ratio of of followers also decreased with an increasing number of synaptic jumps (Fig. 4E). In summary, followers synaptically closest to the source neuron respond most reliably and are the most robust to turnover.

We next asked how long followers last and whether their properties evolve with ongoing plasticity. We divided a period (2,000 s) after reaching steady state into small intervals (100 s) and detected new, lost and remaining followers. In each of these intervals, new followers had lower responding probabilities than those that remained from the previous interval, as well as longer delays, and more synaptic jumps from the source neuron. The distribution of the responding probability of lost followers in every interval overlapped with that of new followers (Fig. 4F), confirming that the overall number of followers in the network remained stable (Fig. 2A). When pooling new followers from all intervals ($n = 7,189$), we observed a skewed distribution of lifetimes (Fig. 4G), with most neurons being classified as followers for a short period. Interestingly, a small proportion (7.3%) of new followers lasted over 1,000 s, much longer than the time constant of the overall decay of followers, $\tau_{seq} = 459$ s (Fig. 4D), suggesting that the network may stabilize some new followers after they are recruited. The responding probability of followers followed a non-monotonic trajectory, first increasing and then decreasing with time, that was common to all followers, independent of their lifetime (Fig. 4H). Some followers displayed remarkably long lifetimes, remaining followers for as long as our simulations. These highly stable followers also showed peak responding probability.

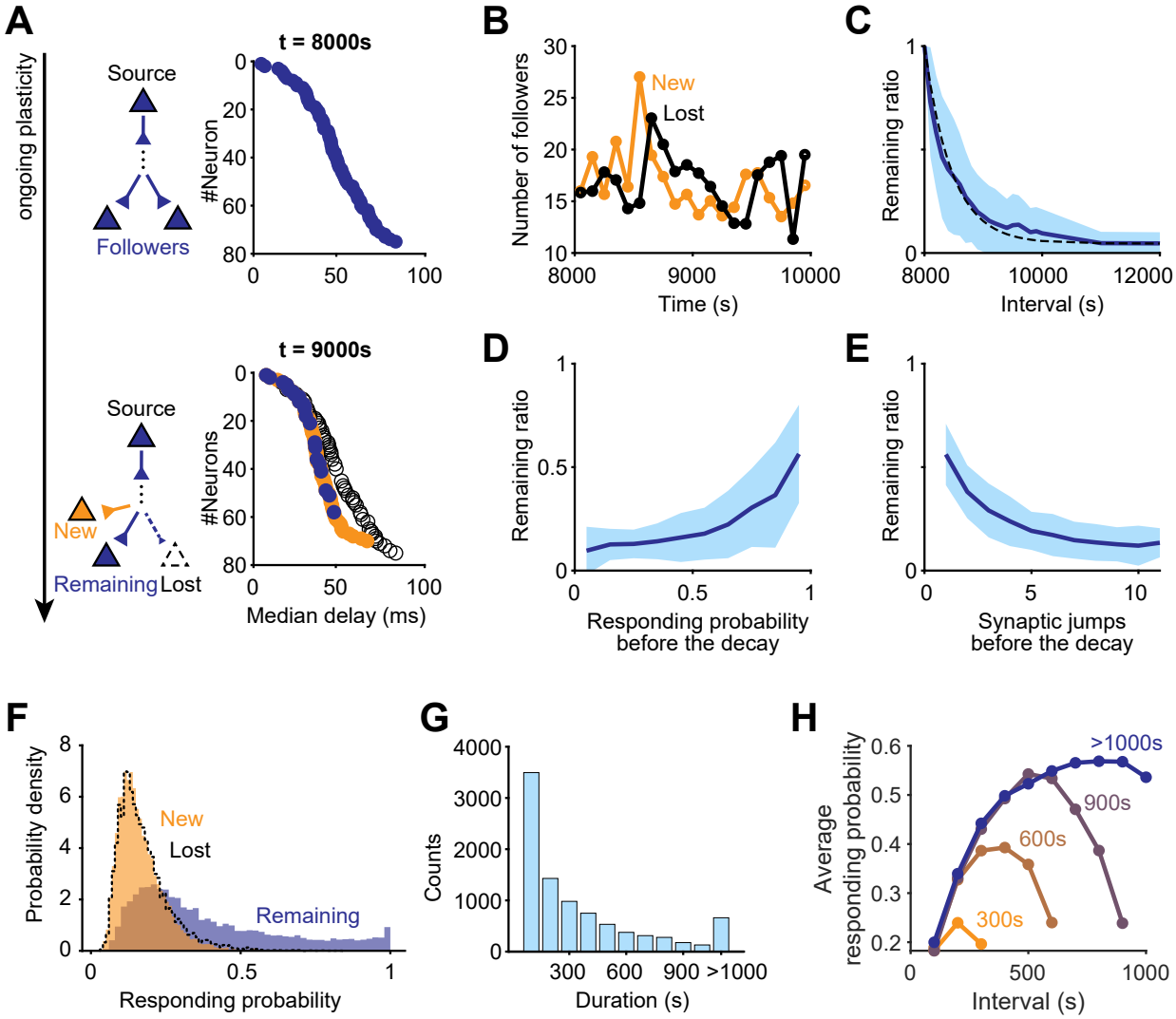

Figure 4. Turnover of followers and sequences. A. Excitatory followers of an example source neuron at two time points. Blue circles indicate common followers at both time points (Remaining). Hollow circles indicate cells classifying as followers earlier but not later (Lost). Orange circles indicate those classifying as followers later but not earlier (New). **B.** Mean number of new and lost followers over 50 sequences in 100 s intervals. **C.** Decay of the probability that a follower continues to classify as a follower after a given interval (pooled over 2,931 followers from 50 sequences, mean±std). Dashed line indicates exponential fit with baseline. **D.** Ratio of remaining followers after 1,000 s as a function of their responding probability (pooled over 24,311 followers from 50 sequences at 8 time points, mean±std). **E.** Same as **D** but as a function of number of synaptic jumps from the source. **F.** Distributions of the responding probability for new, remaining, and lost followers in 100 s intervals. **G.** Distribution of the followers' lifetime. Pooled from followers detected every 100 s from 50 different sequences. **H.** Mean responding probability for different groups of followers, grouped by by their lifetime. Pooled over 2,338 followers from 50 sequences.

In summary, as with synaptic connection distributions, our networks under uncorrelated inputs showed stable global properties and local fluctuations. Single sequences experienced the appearance of new followers and disappearance of old ones so that the overall extent of sequential activity in the network remained constant. While many followers experienced short lifetimes with low responding probabilities,

others could be stabilized in the network, becoming long-lasting and highly responsive followers.

Structured inputs lead to structured connectivity and stable turnover

Our results so far have addressed the dynamics of network structure (Fig. 2, Fig. 3) and its effects on sequential activity (Fig. 4) when the network is subject to uncorrelated inputs. Even under this apparent "noise", we observed features of stability for structures supporting sequential activity (Fig. 2D, Fig. 3D, Fig. 4H). Next we addressed whether structured inputs may affect these structures.

We modeled temporally coherent afferent inputs targeted to groups of neurons to complement our ongoing spontaneous activity. We first defined random groups of neurons (ensembles) in the excitatory population and introduced a structured input pattern with pairwise correlations that sequentially shifted from ensemble to ensemble every 100 s (Fig. 5A). After 10,000 s of simulation, we observed a stable long-tailed distribution of synaptic strengths (Fig. S10A-B). As a result of the structured input, however, strong E-to-E connections concentrated within single ensembles, with very low chance (9.1×10^{-4}) of strong connections between different ensembles (Fig. 5B-C). Consequently, followers were most likely found within the same ensemble (Fig. 5D). Pooling from 126 source neurons, we detected 252 followers in the same ensemble as their source and 155 followers in any other of the remaining 11 ensembles. The percentage of same-ensemble followers (61.9%) was much higher than what would be expected if followers were distributed uniformly (9.1%). Furthermore, same-ensemble followers had significantly higher responding probability than different-ensemble followers (0.47 ± 0.40 vs. 0.25 ± 0.28) and shorter delays (15.7 ± 10.6 ms vs. 24.8 ± 10.8 ms).

Structured inputs not only concentrated strong connections but also made them more stable than those resulting from training under uncorrelated activity (Fig. 5E, blue and gray). Furthermore, while turnover of single strong connections did occur, those decayed strong connections were quickly compensated by new ones in the same ensemble, preserving the high density of strong connections within ensembles and resulting in very stable connectivity (Fig. 5E, pink).

We next asked if these stable structures could be learned by a network that had been previously trained with uncorrelated activity. We first trained a network with unstructured inputs until it reached steady state ($t = 8,000$ s), and then switched to structured inputs (Fig. 5F). We found that the network connectivity adjusted so that strong connections that existed between ensembles disappeared and new strong connections emerged within ensembles. Correspondingly, the percentage of same-ensemble followers rose from 8.3% to 42.9%.

Finally, we asked if these stable structures limited the capacity of the network to adapt to a change in the inputs. We first trained a network with correlated inputs until it reached steady state, and then switched to a new, randomly generated, pattern (Fig. 5G). Note that, since patterns were random and all neurons belonged to some ensemble, the two patterns had a slight overlap. The network re-structured its connectivity to produce sequences corresponding to new ensemble pattern and reached a stable steady state. Correspondingly, the percentage of same-ensemble followers of pattern A dropped from 78.7% to 9.0%, while the percentage of same-ensemble followers of pattern B rose from 5.5% to 68.8%.

In summary, correlated inputs can shape the connectivity that leads to sequences into clusters and stabilize them in our plastic network. Strong connections concentrate between neurons with correlated activity, yielding reliable followers and slowing down turnover. Despite this enhanced stability, the network remains still flexible to accommodate changes in its inputs and produce distinctive sequences that represent them.

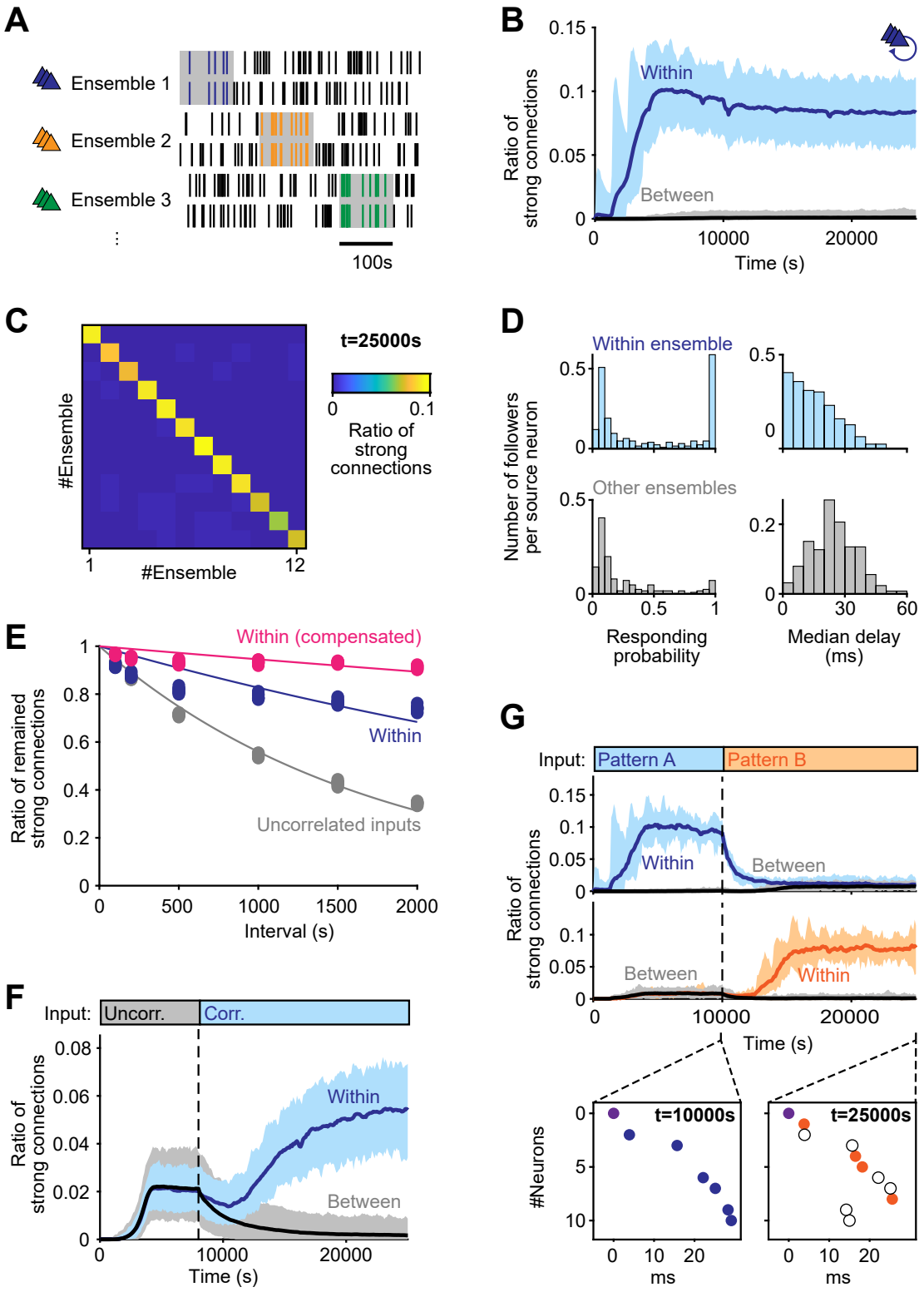

Figure 5. (Caption on the next page.)

Figure 5. Structured inputs lead to structured connectivity and stable turnover. A. Schematic of training protocol. Correlated inputs were sequentially presented to non-overlapping groups (ensembles) of excitatory neurons (color-coded) for 100 s (gray shading). Other neurons received uncorrelated inputs at the same rate. The stimulus cycled throughout the simulation. **B.** Ratio of strong E-to-E connections where pre- and post-synaptic neurons are in the same ensemble (within) or in different ensembles (between), ($n = 10$; mean$\pm$std). **C.** Ratio of strong connections within and between ensembles at steady state ($t = 25,000$ s in B). Most of the strong connections are formed within the correlated ensembles (diagonal). **D.** Distribution of responding probability (left) and median delay (right) of followers in the same ensemble with the source neuron (blue, $n = 155$) or in other ensembles (gray, $n = 97$). **E.** Decay rate of strong E-E connections in the network with and without correlated inputs. Blue: E-to-E connections within ensembles. Gray: Decay in the network with uncorrelated inputs (same as Fig. 2D, blue). Pink: Same as blue but turnover of a connection was not counted if it was replaced by a new connection in the same ensemble. Lines indicate exponential fits ($\tau_{within} = 5,259$ s, $\tau_{uncorr} = 1,721$ s, $\tau_{comp} = 17,761$ s). **F.** Ratio of strong connections, in networks first trained with uncorrelated inputs and then correlated inputs ($n = 10$; mean$\pm$std). **G.** Same as **F** but networks were first trained with one correlated input pattern and then switched to a different correlated input pattern. Top: within and between connections relative to first pattern. Middle: same relative to second pattern. Bottom: Example sequences from the same source two time points. Orange and hollow circles are new and lost followers relative to the first time point.

Temporally structured inputs lead to sequentially organized followers

Our network could produce turnover of sequences in response to unstructured activity and stable sequences in response to structured activation of ensembles of neurons. Next, we asked how the network responded to structured inputs that are themselves temporally structured.

We modeled temporally structured inputs as Poisson spikes received by ensembles of 100 excitatory neurons, one ensemble at a time. This time, however, the inputs were much shorter in duration (10 ms), comparable to the timescale of single neuron dynamics in our model, and shifted quickly from one ensemble to the next without temporal gaps between them (Fig. 6A). Ensembles were ordered temporally and their sequential activation repeated in a circular fashion throughout the simulation.

After 16,000 s of simulation, the network again reached a steady state with a long-tailed distribution of synaptic strengths (Fig. S10C-D). We found that strong connections emerged not only within ensembles (diagonal of the connectivity matrix), but also from one ensemble to the next in the stimulus sequence (sub-diagonal, Fig. 6C). These next-ensemble connections resulted in the extension of sequences over multiple ensembles (Fig. 6D).

Strong connections within the same ensemble and from one ensemble to the next were more stable than strong connections in a network trained with unstructured Poisson inputs (Fig. 6E, blue and gray). As in the case of static ensembles, any strong connection that turned over in a consecutive ensemble pair was quickly compensated by the appearance of a new strong connection in same the ensemble pair. The effective turnover rate therefore was very low, with a time constant longer than our simulations (Fig. 6E, pink). This highly stable connectivity resulted in highly responsive and stable followers: followers in the same ensemble as their source neuron or in the next ensemble had a significantly higher responding probability than any follower in the other 10 ensembles (0.64 ± 0.40 vs. 0.40 ± 0.36 for same-ensemble; 0.53 ± 0.39 vs. 0.40 ± 0.36 for next-ensemble), as well as shorter delays (10.5 ± 9.9 ms vs. 28.0 ± 13.4 ms for same-ensemble; 13.7 ± 8.3 ms vs. 28.0 ± 13.4 ms for next-ensemble), (Fig. 6F).

Finally, we tested if this temporal structure could flexibly reorganize networks with two types of pre-existing structure: that resulting from uncorrelated inputs (Fig. 6G), and that resulting from a different,

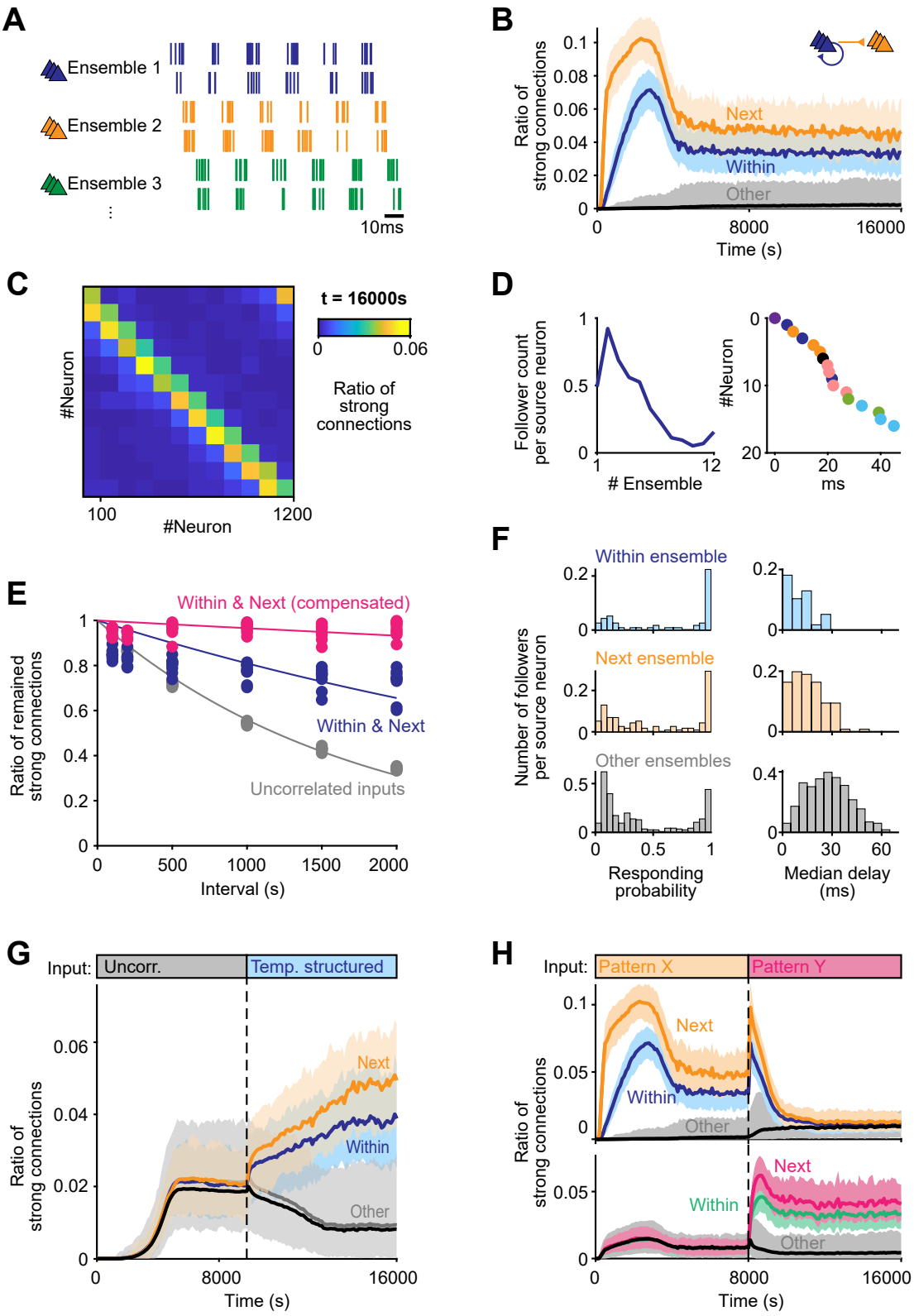

Figure 6. (Caption on the next page.)

Figure 6. Temporally structured inputs lead to sequentially organized followers. A. Schematic of training protocol with temporally structured inputs. Inputs were sequentially presented to non-overlapping groups (ensembles) of 100 excitatory neurons (color-coded) for 10 ms each. Only one ensemble received inputs at a time. Inhibitory neurons received uncorrelated inputs. **B.** Ratio of strong E-to-E connections within the same ensemble (blue), from one ensemble to the next ensemble (orange), and all others (black) ($n = 10$; mean$\pm$std). **C.** Ratio of strong connections within and between ensembles at steady state ($t = 16,000$ s in B). **D.** Left: Average count of followers in different ensembles. Ensemble number is relative to the source neuron: ensemble 1 is the same ensemble, ensemble 2 is the next, etc. Note most followers fall in the immediate next ensemble. Right: example sequence extending over 6 ensembles (different colors). **E.** Decay rate of strong E-E connections. Blue: to a neuron in the same or next ensemble. Pink: same as blue but turnover is counted only if the connection was not replaced by a new one. Black: Decay in the network with uncorrelated inputs (same as Fig. 2D). Lines indicate exponential fits ($\tau_{ee} = 4,738$ s, $\tau_{uncorr} = 1,721$ s, $\tau_{comp} = 28,551$ s). **F.** Distributions of responding probability (left) and median delay (right) of followers in the same ensemble as the source neuron (blue), in the next ensemble (orange), or in other ensembles (gray) ($n = 116$ sequences, $n_{within} = 57$, $n_{next} = 107$, $n_{other} = 326$). **G.** Ratio of strong connections within ensembles, from one ensemble to the next, and anywhere else, in a network first trained with unstructured inputs and then with temporally structured inputs ($n = 10$; mean$\pm$std). **H.** Same as **G** but network was first trained with one pattern and then with a different one ($n = 10$; mean$\pm$std).

random, temporally structured input (Fig. 6H). We first subjected a network to either initial pattern until it reached steady state and then applied a new temporally structured input pattern (Fig. 6A). In both cases, the network quickly reorganized its strong E-to-E connections to the ensemble structure described above (Fig. 6C), resulting in sequences that activated over multiple ensembles and reflected the ordering of the new inputs.

In summary, temporally structured inputs could shape stable sequences that reflect the temporal order of the inputs. The resulting strong connections had a very low turnover ratio, creating a stable backbone of propagation that sequentially linked multiple groups of neurons. Nonetheless, this stable configuration was also flexible enough to adapt to changes in the input patterns.

Discussion

Here, we investigated how repeating sequences of spikes may arise and change under continuous plasticity. We built a spiking neural network composed of recurrently connected excitatory and inhibitory neurons with biologically-plausible synaptic plasticity rules (Fig. 1A). We found the network spontaneously reached lognormal weight distribution and structures of connectivity that made it prone to produce sequences even under the complete absence of structured stimuli (Fig. 1C-G). Although the statistics of these structures were stable, particular synaptic weights and sequences evolved due to the constant turnover of connections (Fig. 2, Fig. 4). Still, the timescales of turnover were longer for features of connectivity that supported sequences when compared to random connectivity (Fig. 2D-E, Fig. 3). This lower volatility could be further reduced when the network was subjected to external structured stimuli (Fig. 5E, Fig. 6E). Indeed, the network could sustain representations for long periods of time while at the same time remaining sufficiently flexible to adapt to changes in the stimulus (Fig. 5G, Fig. 6G).

Plasticity rules that promote sequential activity

Our results, with sequential activity emerging from a random network, lend support to STDP being the main actor in producing sequences of spikes, as long as it is combined with stabilizing mechanisms such as weight normalization and intrinsic plasticity [38, 53, 55]. Together, these rules give rise to stable long-tailed weight distributions of excitatory connections (Fig. 1C) that then drive sequential activity (Fig. 1E, [35, 50, 52]). This particular combination of plasticity rules avoids the presence of dominant excitatory neurons that concentrate all strong connections (i.e., hub neurons [62–64]). Instead, strong connections are spread across the network, enabling long sequences that could start almost everywhere (Fig. 1D). Beyond single sequences, we also studied connectivity structures and found over-representation of motifs that promote sequential activation (fan-in/out motifs), consistent with experimental evidence on the routing of neuronal activity [59].

Beyond excitation, our work also involved plasticity of I-to-E connections through a symmetric iSTDP rule, resulting in a balance of excitation and inhibition (Fig. 1A, [34]). In consequence, excitatory neurons that initiate sequences receive strong feedback inhibition after the onset of the sequence (Fig. S5), as observed experimentally [7]. This is the result of inhibitory neurons starting to fire after multiple excitatory neurons have been activated as the sequence extends. (Fig. 1F). By reducing the activation of excitatory neurons in the sequence and surrounding neurons, this form of negative feedback mechanism might limit the growth of excitatory connections and contributing to their eventual turnover [65].

The stability of these long-tailed distributions of excitatory connections neither depended on the presence of structured input, nor was it impaired by it. Our simulations with correlated and temporally-structured inputs did not affect the statistics of our excitatory weight distributions (Fig. S10). The presence of structured input instead resulted in additional structures within the connectivity matrix. Correlated inputs over long timescales produced groups of recurrently connected neurons similar to neuronal “assemblies” (Fig. 5C, [35, 40]). Fast inputs with temporal structure on the other hand, produced cross-assembly connections similar to “neuronal clocks” (Fig. 6C, [48]). In both cases, we observed sequential activity of reliable followers and a slow turnover of the connectivity that produces them, highlighting the robustness and flexibility of these plasticity rules.

Long-tailed distributions of synaptic efficacies as well as sequential activation of neurons are widely observed phenomena across multiple brain areas and species [57, 58, 60, 62, 65–67]. Theoretical studies with different degrees of biological realism have proposed links between these two elements [35, 50, 52, 68, 69]. Our results from random networks under random input contribute to this link and propose the role of specific plasticity rules to explain the widespread presence of both, long-tailed distributions and spiking sequences, in the brain.

Turnover of representations?

Spiking sequences have been proposed to be an intrinsic feature of the brain, rather than a reflection of sequential input [3]. The brain can use these structures during learning to anchor representations. Our work with random connectivity and random input producing sequences provides a mechanism for the emergence of this representational substrate. However, despite the robust statistics of our networks, we found a constant turnover of synaptic connections (Fig. 2) that resulted in a constant turnover of followers (Fig. 4) and thus the eventual alteration of any given sequence. If sequences are often observed in sensory, motor and navigational cortices, and are meant to bind representations, how might this turnover affect the

encoding of external stimuli, actions or places?

An increasing body of experimental evidence suggests that representations in the brain might be subject to a slow "drift", where patterns of neuronal activity correlate with task features in the short timescale, but the overall representations radically change in the long term [8]. Drift has been reported in multiple brain regions, such as mice posterior parietal cortex (PPC, [70]), mice visual cortex [10, 11], the hippocampus of mice and rats [16, 71], mice olfactory cortex [72], as well as *Drosophila* mushroom body [73]. The sequences that we describe here present sudden drops of single followers but overall slow changes of the whole sequence (Fig. 4) and thus seem suitable candidates to underlie some of these drifting representations. Recent work in the hippocampus suggests that slow drift of place representation at the scale of population codes may be the reflection of sudden changes of place fields at the level of single neurons, which is very consistent with our modeling results [74].

To deal with how a downstream area might decode a drifting representation, theoretical studies propose plastic readouts that can adjust to the encoding as long as the timescale of the drift is slower than the timescale of the decoding [75, 76]. Our sequences present a drift of the neurons involved at multiple timescales: more remote followers drop out more quickly while closer followers are more stable (Fig. 4), resulting in a slow drift in the representation at the scale of the whole sequence. Furthermore, since most neurons in our networks could elicit a sequence, multiple sequences may run in parallel [50], which could extend even further the stability of the representations when considering the whole population. Our work with structured input strongly supports this possibility: when considering any strong connection among the followers within an ensemble, turnover timescales became longer than our simulations (Fig. 5E, Fig. 6E, pink).

Interestingly, in the mouse primary visual cortex, the representations corresponding to some simple and basic visual stimuli (e.g., gratings) are very stable, while the representations of more natural and complex visual stimuli are more unstable [11]. This form of complexity-dependent drift seems consistent with the different turnover dynamics we observe between early (stable) followers and late (unstable) followers (Fig. 4). Previous modeling work showed that contextual network activation determines the dynamic activation of later followers, suggesting a higher degree of selectivity of later than earlier followers [50]. Our results would thus be consistent with early neurons in the sequence representing simpler stimuli, possibly receiving direct thalamic inputs, while later neurons representing more complex stimuli. These later, complex, representations would be more amenable to drift because they rely on the activation (and stability) of multiple strong connections within the recurrent circuit (Fig. 4E). Since natural environments likely present a large variety of slightly different stimuli, later followers with very high stimulus selectivity may activate very rarely, and, consequently, may be more prone to turnover under our plasticity rules, resulting in a stronger drift in terms of representation. This view aligns well with prior theoretical frameworks of sparse coding, which aimed to explain why the large majority of neurons are mostly silent [77].

Although representations of sequential activity primarily rely on strong connections, weak connections may also be highly relevant for their plasticity-driven turnover. The high volatility of weak connections in our simulations (2E) suggests a quick mechanism for network computations: If weak connections are particularly susceptible to plastic changes due to the network dynamics, they may be ideally positioned to implement fast flexibility into the network. Indeed, weak connections are likely to play a role in implementing competition and cooperation across multiple sequences [50]. Under this view, reactivation of sequences under changing inputs will be first subject to the modulation of weak connectivity and may, on a longer timescale, result in the reorganization of the more stable backbone of strong connections.

Finally, although our model network may capture features of stimulus representational drift, it has a limited memory capacity. Indeed, while changing of input patterns can be seen as a feature of flexible adaptation to changing stimulus statistics (Fig. 5F-G, Fig. 6G-H), it can also be interpreted as a volatile memory issue, commonly known as "catastrophic forgetting" [78]. A possible avenue of future research to address this issue may lie on the suitable dynamics of learning of a readout layer, as described above [75, 76], or on the mixed presentation of patterns, similar to previous modeling work on hippocampal sequence replay [79].

Methods

Neuronal model

We used the adaptive exponential integrate-and-fire neuronal model (AdEx, [51]) for both excitatory and inhibitory neurons in the network. The membrane potential dynamics of the neurons were governed by the following equation:

$$C_m \frac{\mathrm{d}V}{\mathrm{d}t} = -g_L(V - E_L) - g_e(V - E_e) - g_i(V - E_i) + I_{spike}(V) - u + I(t) + \xi(t), \tag{1}$$

where C_m is the membrane capacitance, g_L is the leaky conductance, g_e and g_i are the conductances of the excitatory and inhibitory channels. E_L, E_e and E_i are reversal potentials of the leaky, excitatory, and inhibitory channels, respectively. $I(t)$ is the background current following a Gaussian distribution with the mean μ_{wn} and the standard deviation σ_{wn}. It is resampled for every interval τ_{wn}. $\xi(t)$ is the Poisson input representing spontaneous activity or input from other parts of the brain not included in the model. We formulated this as a combination of Dirac's delta functions of time with amplitude ξ_{ext}

$$\xi(t) = \xi_{ext} \sum_i \delta(t - t_i), \tag{2}$$

and the time points $\{t_i\}$ are sampled from an exponential distribution with time constant τ_{ext}. u is an adaptation term following the differential equation below:

$$\tau_u \frac{\mathrm{d}u}{\mathrm{d}t} = -a_u(V - E_L) + b_u \delta(t - t_{spike}) - u. \tag{3}$$

$I_{spike}(V)$ is an additional exponential function of the membrane potential V to simulate the spiking process. It can be written as

$$I_{spike}(V) = g_L \Delta T \exp\left(\frac{V - V_{th}}{\Delta T}\right), \tag{4}$$

where V_{th} is the firing threshold and ΔT is a slope parameter which controls the steepness of the membrane potential trace just before a spike. The spiking time points of one neuron are determined as the time steps when the membrane potential exceeds V_{peak}. After a spike, the membrane potential is reset to V_{reset}.

The excitatory and inhibitory channels, g_e and g_i, are determined by the incoming synaptic weights from

excitatory and inhibitory neurons, respectively. They can be formulated as

$$\frac{\mathrm{d}g_e}{\mathrm{d}t} = -\frac{g_e}{\tau_e} + \sum_{i,j} w_i \delta(t - t_{ij}), \tag{5}$$

$$\frac{\mathrm{d}g_i}{\mathrm{d}t} = -\frac{g_i}{\tau_i} + \sum_{k,j} w_k \delta(t - t_{kj}), \tag{6}$$

where the index i corresponds to presynaptic excitatory neurons and w_i denotes the excitatory incoming synaptic weights from them, while the index k refers to presynaptic inhibitory neurons and their associated connections. The index j denotes the spike timings and t_{ij} represents the spike train of the presynaptic neuron i.

Table 1. Parameters in the neuronal model

Parameter	Description	Value
C_m	Membrane capacitance of the neuron	240 pF
g_L	Leaky conductance of the neuron	4.19 nS
E_L	Reversal potential of the leaky channel	-70.6 mV
E_e	Reversal potential of the excitatory channel	10 mV
E_i	Reversal potential of the inhibitory channel	-75 mV
μ_{wn}	Mean of the background inputs	62.5 pA
σ_{wn}	Standard deviation of the background inputs	21.4 pA
τ_{wn}	Interval between two sampling of the background inputs	1 ms
ξ_{ext}	Amplitude of the external Poisson inputs	1 mV
τ_{ext}	Time constant of the external Poisson inputs	3 ms
a_u	Conductance of the adaptive channel	4 nS
b_u	Additional adaptive current when the neuron spikes	80.5 pA
τ_u	Time constant of adaptation	144 ms
ΔT	Slope constant of the spiking current $I_{spike}(V)$	2 ms
V_{th}	Firing threshold of I neurons, and the initial firing threshold of E neurons	-50.4 mV
V_{reset}	Reset potential	-60 mV
V_{peak}	Peak potential to identify spikes	0 mV
τ_e	Time constant of the excitatory channel	1.1 ms
τ_i	Time constant of the inhibitory channel	1.1 ms
dt	Simulation time step	0.1 ms

Network model

The model neural network consisted of 1,200 excitatory (E) and 240 inhibitory (I) AdEx neurons [51] with sparse connections between all neuron types (Fig. 1A, Table 2). Initial connectivity was random and homogeneous, with weak strengths unable to cause a postsynaptic spike with a single presynaptic one. E-to-E and I-to-E connections were plastic, while E-to-I and I-to-I connections were static. The model did not include structural plasticity [80], such that no new connections were created or eliminated even if some of them decreased to zero due to plasticity. The sum of incoming E-to-E synaptic weights for each postsynaptic neuron was kept constant at T^{ee}. Similarly, the sum of all the incoming I-to-E, E-to-I, and I-to-I connections for one neuron, equals to T^{ie}, T^{ei}, and T^{ii}, respectively. In this initial network, the maximal effective E-to-E weight was ~ 0.5, much lower than the maximum after plasticity (~ 10) and the estimated threshold to trigger a postsynaptic spike (~ 2.5). A synaptic delay of 1.5 ms was modeled for all connections.

Table 2. Parameters in the network model

Parameter	Description	Value
p_{ee}	Connection probability from E to E	0.06
p_{ei}	Connection probability from E to I	0.19
p_{ie}	Connection probability from I to E	0.2
p_{ii}	Connection probability from I to I	0.11
T^{ee}	Sum of incoming E-to-E connections	297 nS
T^{ei}	Sum of incoming E-to-I connections	1012 nS
T^{ie}	Sum of incoming I-to-E connections	643 nS
T^{ii}	Sum of incoming I-to-I connections	373 nS
d_{syn}	Synaptic delay	1.5 ms

Plasticity model

The plasticity mechanisms in our model included four different components: excitatory STDP for E-to-E connections, inhibitory STDP for I-to-E connections, synaptic normalization, and intrinsic plasticity for excitatory neurons (Fig. 1A).

1. Excitatory STDP (eSTDP)

The change of the synaptic weight of an E-to-E connection was determined as

$$\Delta w_{ee} = \begin{cases} A_+ \text{exp}\left(\frac{-\Delta t}{\tau_+}\right), & \Delta t > 0 \\ -A_- \text{exp}\left(\frac{\Delta t}{\tau_-}\right), & \Delta t < 0 \end{cases} \tag{7}$$

for a pair of pre- and postsynaptic spikes separated by a temporal difference of $\Delta t = t_{post} - t_{pre}$.

2. Inhibitory STDP (iSTDP)

The change of the synaptic weight of an I-to-E connection was determined as

$$\Delta w_{ie} = A_i \text{ exp}\left(-\frac{|\Delta t|}{\tau_i}\right) \tag{8}$$

for a pair of pre- and postsynaptic spikes separated by a temporal difference between of $\Delta t = t_{post} - t_{pre}$. Additionally, whenever there was a presynaptic spike, a weight change was applied:

$$\Delta w_{ie} = -A_{LTD} \tag{9}$$

3. Weight normalization

Pre- and postsynaptic weight normalizations were applied to both E-to-E and I-to-E connections. Postsynaptic normalization for E-to-E connections ensured that the sum of incoming excitatory synaptic weights for each postsynaptic excitatory neuron remained constant at T^{ee}, using the updating rule below:

$$w_{ji}^{ee} \rightarrow \frac{T^{ee}}{\sum_j w_{ji}^{ee}}. \tag{10}$$

Presynaptic normalization kept the sum of outgoing synaptic weights from excitatory neuron i at S_i^{ee}, using

the updating rule

$$w_{ji}^{ee} \to \frac{S_i^{ee}}{\sum_i w_{ji}^{ee}}. \tag{11}$$

Similarly, for I-to-E connections, the sum of incoming inhibitory synaptic weights for each postsynaptic excitatory neuron was kept at T^{ie}, while the sum of outgoing synaptic weights from inhibitory neuron i remained constant at S_i^{ie}, using the rule

$$w_{ji}^{ie} \to \frac{T^{ie}}{\sum_j w_{ji}^{ie}} \tag{12}$$

and

$$w_{ji}^{ie} \to \frac{S_i^{ie}}{\sum_i w_{ji}^{ie}}. \tag{13}$$

4. Intrinsic plasticity for excitatory neurons

All E neurons were subject to intrinsic plasticity, adjusting their firing thresholds to match a universal target firing rate for all neurons. If an E neuron fired more than the target rate, its firing threshold would increase to reduce the firing rate back to the target, and vice versa, as follows:

$$\frac{\mathrm{d}V_{th,i}}{\mathrm{d}t} = \eta_{IP}\left(\delta(t - t_{spike}^i) - r_t\right) \tag{14}$$

where $V_{th,i}$ is the firing threshold of neuron i, t_{spike}^i is the spike time of neuron i. r_t is the target firing rate and η_{IP} is the rate of intrinsic plasticity.

Due to the dynamic firing threshold of excitatory neurons and in order to quantify the real impact of synapses, we defined the "effective weight" W_{eff}, which is the synaptic weight W divided by the distance from the resting potential V_0 to the firing threshold V_{th}, i.e.,

$$W_{\text{eff}} = \frac{W}{V_{th} - V_0}. \tag{15}$$

Here the resting potential is defined as the membrane potential when only the background inputs $I(t)$ presents.

Table 3. Parameters in the plasticity model

Parameter	Description	Value
A_+	LTP amplitude in eSTDP	1.6 nS
A_-	LTD amplitude in eSTDP	0.32 nS
A_i	LTP amplitude in iSTDP	1.6 nS
A_{LTD}	LTD amplitude in iSTDP	0.0432 nS
τ_+	LTP time constant in eSTDP	15 ms
τ_-	LTD time constant in eSTDP	30 ms
τ_i	LTP time constant in iSTDP	15 ms
η_{IP}	Update rate in the intrinsic plasticity	0.05 mV
r_t	Target firing rate of excitatory neurons	0.45 Hz
V_0	Resting membrane potential (calculated from simulations)	-63 mV

Sequence extraction

To start a sequence, we first shut down all the plasticity mechanisms operating on the network, and then we forced a neuron to spike. This forced neuron is called the "source neuron" of the sequence. The frequency of the Poisson input $\xi(t)$ was reduced (τ_{ext} = 4 ms) to compensate for the forced spike.

We ran a testing paradigm that lasted 43 seconds, with the first 3 s for the network to obtain stable activity. Then the first triggered spike occurred at $t = 3.1$ s. After that, a spike was triggered in the same source neuron for every 400 ms, resulting in 100 trials of the sequence. In each trial, We calculated for every neuron the "firing rate before stimulation" r_1 as the firing rate in the 100 ms window just before the triggered spike, and the "firing rate after stimulation" r_2 as the firing rate in the 300 ms window just after the triggered spike. We repeated this paradigm for 10 times and generated $M = 1,000$ pairs of r_1 and r_2.

Meanwhile, we used $\langle r_1 \rangle$ and $\langle r_2 \rangle$ (averaged over all neurons and the $M = 1,000$ trials) that we obtained above to build a null model with only one neuron and $M' = 10,000$ spike triggering. This neuron fired with Poisson statistics. Consistent with the paradigm above, in every 100 ms window before the spike triggering, the neuron fired at the firing rate $\langle r_1 \rangle$. In every 300 ms window after the spike triggering, the neuron fired at the firing rate $\langle r_2 \rangle$. This allowed us to have a null distribution of r_1 and r_2 with $M' = 10,000$ samples.

We defined the "firing rate modulation" (Δr) as the difference between r_2 and r_1, i.e., $\Delta r = r_2 - r_1$. Every pair of r_1 and r_2 could lead to one observation of Δr. To reduce noise, we divided the $M = 1,000$ observations of Δr in the simulation and $M' = 10,000$ observations of Δr in the null model into 10 equal parts. In each part, we calculated the null model's 95th percentile of Δr. For one specific neuron, only if its average Δr was higher than the 95th percentile of the null model in all the 10 parts could it be identified as a follower.

To calculate the responding probability, delay, and jitter(Fig. S3C-D), for every identified follower, in each of the $M = 1,000$ trials of spike triggering, we searched for its first spike after the externally triggered spike. If no spike was detected within a 300 ms window after the spike triggering, we considered the follower unresponsive to the source neuron for that trial. If a spike was found, the elapsed time from the triggered spike was recorded as the delay. If a follower responded to the source neuron in M^* out of the $M = 1,000$ trials, its responding probability was then M^*/M (Fig. 1E). A total of M^* delays were recorded, with the median calculated as the median delay, and the standard deviation defined as the jitter.

After extracting the sequences generated from all excitatory neurons, we estimated the minimal effective weight required to trigger a follower. The threshold was estimated to be 2.5 nS/mV (Fig. S1C) and determined as the criterion to classify strong connections.

Decay of connections

When calculating the decay rate of connections at a given time interval, we retrospectively took multiple snapshots of the network (up to 11) starting from the end of the simulation, within the period when the network was in a steady state, with the specified time interval between each two snapshots. Then we calculated the ratio of remaining connections from one snapshot to the next and averaged these ratios across all snapshots, resulting in one data point corresponding to one instantiation of the network (Fig. 2D). For example, for a 2,000 s interval, we took snapshots at 16,000 s, 14,000 s, 12,000 s, 10,000 s, and 8,000 s, assuming the network reached the steady state after $t = 8,000$ s. For a 100 s interval, snapshots were taken at 16,000 s, 15,900 s, ..., 15,100 s, 15,000 s, covering the last ten 100 s intervals in the 16,000 s simulation. The decay of motifs were calculated following the same procedure.

The turnover time constant τ of connections or motifs was fitted using an exponential function:

$$r = a * \exp(-t/\tau) + 1 - a, \tag{16}$$

where r is the remaining ratio and t is the time interval. If there was no baseline in the exponential function, we fixed $a = 1$ in the fitting.

Motif analysis

The ratio of motif was calculated as the number of motifs found in the network (N) divided by the total number of all possible sites where a motif can emerge (N_0). The numbers of sites were different for the multiple motif types we were investigating and were dependent on the number of neurons and the connection probability p_{ee}.

For the linear chains,

$$N_0 = P_3^{N_e} p_{ee}^2 = p_{ee}^2 N_e(N_e - 1)(N_e - 2) \tag{17}$$

where P is the permutation number.

For the convergence and divergence motif,

$$N_0' = N_e \binom{N_e - 1}{2} p_{ee}^2 = \frac{1}{2} p_{ee}^2 N_e(N_e - 1)(N_e - 2). \tag{18}$$

For the fan-in/out motif,

$$N_0'' = N_e P_2^{N_e - 1} p_{ee}^3 = p_{ee}^3 N_e(N_e - 1)(N_e - 2). \tag{19}$$

Given a specific ratio of strong connection p_0, we could calculate the ratio of motif in a random network, which was compared to the ratio of motif in our simulation (Fig. 3C). For the linear chains, the random ratio was

$$\frac{1}{N_0}(p_0 p_{ee})^2 (1 - p_0 p_{ee})^4 N_e(N_e - 1)(N_e - 2) = p_0^2 (1 - p_0 p_{ee})^4. \tag{20}$$

Similarly, for the convergence and divergence motif, the ratio was

$$\frac{1}{N_0'}(p_0 p_{ee})^2 (1 - p_0 p_{ee})^4 N_e(N_e - 1)(N_e - 2)/2 = p_0^2 (1 - p_0 p_{ee})^4. \tag{21}$$

For the fan-in/out motif, the ratio was

$$\frac{1}{N_0''}(p_0 p_{ee})^3 (1 - p_0 p_{ee})^3 N_e(N_e - 1)(N_e - 2) = p_0^3 (1 - p_0 p_{ee})^3. \tag{22}$$

Follower turnover

When analyzing follower turnover based on responding probabilities, delays, and synaptic jumps (Fig. 4D, 4E, and S9A), we selected an interval of 1000 s and took 9 snapshots of the network from $t = 8,000$ s to $t = 16,000$ s, generating 8 intervals to calculate the remaining ratio of followers. Taking Fig. 4D as an example, we selected 50 sequences and went over these 8 intervals, calculating the remaining ratio of the

followers with given responding probability. This yielded 400 ratios, which were averaged using the number of followers in each snapshot as weights.

Correlated and temporally shifting inputs

Different parameters of the neuronal model were used when modeling these inputs (Fig. 5 and 6). Their values are listed below.

Table 4. Correlated inputs (Fig. 5)

Parameter	Description	Value
T_{corr}	Period in which correlated inputs are given to an ensemble	100 s
T_{gap}	Period in which no correlated inputs are given (between two periods with correlation)	5 s
ρ_{corr}	Correlation of correlated external inputs	1.0 (fully correlated)
$\xi_{ext,e}$	Amplitude of external inputs to E neurons	20 mV
$\tau_{ext,e}$	Time constant of external inputs to E neurons	400 ms
$\xi_{ext,i}$	Amplitude of external inputs to I neurons	20 mV
$\tau_{ext,i}$	Time constant of external inputs to I neurons	300 ms

Table 5. Temporally shifting inputs (Fig. 6)

Parameter	Description	Value
T_{corr}	Period in which correlated inputs are given to an ensemble	10 ms
T_{gap}	Period in which no correlated inputs are given (between two periods with correlation)	0
$\xi_{ext,e}$	Amplitude of external inputs to E neurons	1 mV
$\tau_{ext,e}$	Time constant of external inputs to E neurons	0.6 ms
$\xi_{ext,i}$	Amplitude of external inputs to I neurons	1 mV
$\tau_{ext,i}$	Time constant of external inputs to I neurons	3 ms
r_t	Target firing rate of E neurons	0.7 s

Entropy and rank correlation of the sequence

Following the same calculation as in [7], the entropy of a sequence was defined as

$$H_k = -\sum_i P_{ik} \log P_{ik} \tag{23}$$

where P_{ik} is the probability for follower i to be the kth to fire in the sequence. In a totally random sequence with n followers, $P_{ik} = 1/n$ for all the followers and the entropy for any k equals to

$$H_0 = -n * \frac{1}{n} \log \frac{1}{n} = \log n, \tag{24}$$

allowing us to define the normalized entropy as H_k/H_0. We took the $n = 135$ sequences in Fig. S1, calculated their normalized entropy, and then created 10 shuffled sequences for each of them (1350 in total) as a null model (Fig. S3A).

To calculate the rank correlation of sequences (Fig. S3B), we first defined an order matrix for every trial

in which a spike was triggered. Specifically, for trial k, the order matrix $O_k(i,j)$ was defined as

$$O_k(i,j) = \begin{cases} 1, & \text{follower } i \text{ fired prior to follower } j \\ -1, & \text{follower } j \text{ fired prior to follower } i \\ 0, & \text{one of follower } i \text{ and follower } j \text{ didn't fire} \\ 0, & \text{the difference of their firing time was smaller than 2 ms} \end{cases} \tag{25}$$

Then we defined

$$S_{k,l}(i) = \langle O_k(i,j)\, O_l(i,j) \rangle_{j \neq i}. \tag{26}$$

As a result, a positive $S_{k,l}(i)$ means the firing orders of follower i relative to other followers in trial k and trial l were similar. A negative $S_{k,l}(i)$ means the firing orders were reversed. Then we could calculate the rank correlation for neuron i as

$$r(i) = \langle S_{k,l}(i) \rangle_{k,l}. \tag{27}$$

Hub neurons

In the network that generated hub neurons (Fig. S7), we removed presynaptic normalization and intrinsic plasticity. We also used some different parameters listed below.

Table 6. Hub neurons

Parameter	Description	Value
A_+	LTP amplitude in eSTDP	0.4 nS
A_-	LTD amplitude in eSTDP	0.08 nS
A_i	LTP amplitude in iSTDP	0.4 nS
A_{LTD}	LTD amplitude in iSTDP	0
ξ_{ext}	Amplitude of external Poisson inputs (only for Fig. S7D)	0

Acknowledgments

This work was supported by funding from Max Planck Society and the European Research Council (ERC) under the European Union's Horizon 2020 research and innovation program (Grant agreement No. 804824). We thank group members of the 'Computation in Neural Circuits' group for discussions and readings of the manuscript.

Author contributions

S.S., J.L.R., and J.G. conceived the research. S.S. developed the model and performed the simulations. S.S., J.L.R., and J.G. wrote the manuscript.

Competing interests statement

The authors declare no competing interests.

References

[1] R. H. Hahnloser, A. A. Kozhevnikov, and M. S. Fee, “An ultra-sparse code underlies the generation of neural sequences in a songbird,” *Nature*, vol. 419, pp. 65–70, 2002.

[2] T. J. Davidson, F. Kloosterman, and M. A. Wilson, “Hippocampal Replay of Extended Experience,” *Neuron*, vol. 63, no. 4, pp. 497–507, 2009.

[3] G. Buzsáki and D. Tingley, “Space and Time: The Hippocampus as a Sequence Generator,” *Trends in Cognitive Sciences*, vol. 22, no. 10, pp. 853–869, 2018.

[4] A. Luczak, P. Barthó, S. L. Marguet, G. Buzsáki, and K. D. Harris, “Sequential structure of neocortical spontaneous activity in vivo,” *Proceedings of the National Academy of Sciences of the United States of America*, vol. 104, no. 1, pp. 347–352, 2007.

[5] F. Pulvermüller and Y. Shtyrov, “Spatiotemporal signatures of large-scale synfire chains for speech processing as revealed by MEG,” *Cerebral Cortex*, vol. 19, no. 1, pp. 79–88, 2009.

[6] C. D. Harvey, P. Coen, and D. W. Tank, “Choice-specific sequences in parietal cortex during a virtual-navigation decision task,” *Nature*, vol. 484, no. 7392, pp. 62–68, 2012.

[7] M. Hemberger, M. Shein-Idelson, L. Pammer, and G. Laurent, “Reliable Sequential Activation of Neural Assemblies by Single Pyramidal Cells in a Three-Layered Cortex,” *Neuron*, vol. 104, no. 2, pp. 353–369.e5, 2019.

[8] L. N. Driscoll, L. Duncker, and C. D. Harvey, “Representational drift: Emerging theories for continual learning and experimental future directions,” *Current Opinion in Neurobiology*, vol. 76, p. 102609, 2022.

[9] M. E. Rule, T. O’Leary, and C. D. Harvey, “Causes and consequences of representational drift,” *Current Opinion in Neurobiology*, vol. 58, pp. 141–147, 2019. Computational Neuroscience.

[10] D. Deitch, A. Rubin, and Y. Ziv, “Representational drift in the mouse visual cortex,” *Current Biology*, vol. 31, no. 19, pp. 4327–4339.e6, 2021.

[11] T. D. Marks and M. J. Goard, “Stimulus-dependent representational drift in primary visual cortex,” *Nature Communications*, vol. 12, no. 1, pp. 1–16, 2021.

[12] C. E. Schoonover, S. N. Ohashi, R. Axel, and A. J. Fink, “Representational drift in primary olfactory cortex,” *Nature*, vol. 594, no. 7864, pp. 541–546, 2021.

[13] J. O’keefe and L. Nadel, *The hippocampus as a cognitive map*. Oxford university press, 1978.

[14] K. I. Blum and L. F. Abbott, “A Model of Spatial Map Formation in the Hippocampus of the Rat,” *Neural Computation*, vol. 8, pp. 85–93, 01 1996.

[15] C. A. Barnes, M. S. Suster, J. Shen, and B. L. McNaughton, “Multistability of cognitive maps in the hippocampus of old rats,” *Nature*, vol. 388, p. 272–275, July 1997.

[16] Y. Ziv, L. D. Burns, E. D. Cocker, E. O. Hamel, K. K. Ghosh, L. J. Kitch, A. E. Gamal, and M. J. Schnitzer, "Long-term dynamics of ca1 hippocampal place codes," *Nature Neuroscience*, vol. 16, p. 264–266, Feb. 2013.

[17] I. I. Low, A. H. Williams, M. G. Campbell, S. W. Linderman, and L. M. Giocomo, "Dynamic and reversible remapping of network representations in an unchanging environment," *Neuron*, vol. 109, no. 18, pp. 2967–2980.e11, 2021.

[18] K. Immelmann, "Song development in the zebra finch and other estrilid finches," in *Bird vocalizations* (R. A. Hinde, ed.), pp. 61–74, New York: Cambridge University Press, 1969.

[19] A. Leonardo and M. Konishi, "Decrystallization of adult birdsong by perturbation of auditory feedback," *Nature*, vol. 399, p. 466–470, June 1999.

[20] G. B. Keller and R. H. R. Hahnloser, "Neural processing of auditory feedback during vocal practice in a songbird," *Nature*, vol. 457, p. 187–190, November 2008.

[21] M. Elmaleh, D. Kranz, A. C. Asensio, F. W. Moll, and M. A. Long, "Sleep replay reveals premotor circuit structure for a skilled behavior," *Neuron*, vol. 109, pp. 3851–3861.e4, December 2021.

[22] H. Simpson and D. Vicario, "Brain pathways for learned and unlearned vocalizations differ in zebra finches," *The Journal of Neuroscience*, vol. 10, p. 1541–1556, May 1990.

[23] D. S. Vicario and H. B. Simpson, "Electrical stimulation in forebrain nuclei elicits learned vocal patterns in songbirds," *Journal of Neurophysiology*, vol. 73, p. 2602–2607, June 1995.

[24] A. Ter Maat, L. Trost, H. Sagunsky, S. Seltmann, and M. Gahr, "Zebra finch mates use their forebrain song system in unlearned call communication," *PLoS ONE*, vol. 9, p. e109334, Oct. 2014.

[25] A. G. Hile, T. K. Plummer, and G. F. Striedter, "Male vocal imitation produces call convergence during pair bonding in budgerigars, melopsittacus undulatus," *Animal Behaviour*, vol. 59, no. 6, pp. 1209–1218, 2000.

[26] D. Z. Jin and A. A. Kozhevnikov, "A compact statistical model of the song syntax in bengalese finch," *PLOS Computational Biology*, vol. 7, pp. 1–19, 03 2011.

[27] J. E. Markowitz, E. Ivie, L. Kligler, and T. J. Gardner, "Long-range order in canary song," *PLoS Computational Biology*, vol. 9, p. e1003052, May 2013.

[28] E. Abs, R. B. Poorthuis, D. Apelblat, K. Muhammad, M. B. Pardi, L. Enke, D. Kushinsky, D.-L. Pu, M. F. Eizinger, K.-K. Conzelmann, I. Spiegel, and J. J. Letzkus, "Learning-related plasticity in dendrite-targeting layer 1 interneurons," *Neuron*, vol. 100, pp. 684–699.e6, Nov. 2018.

[29] C. C. H. Petersen, "Sensorimotor processing in the rodent barrel cortex," *Nature Reviews Neuroscience*, vol. 20, p. 533–546, July 2019.

[30] L. A. Kirkby, G. S. Sack, A. Firl, and M. B. Feller, "A role for correlated spontaneous activity in the assembly of neural circuits," *Neuron*, vol. 80, p. 1129–1144, Dec. 2013.

[31] Y. Tezuka, K. M. Hagihara, K. Ohki, T. Hirano, and Y. Tagawa, "Developmental stage-specific spontaneous activity contributes to callosal axon projections," *eLife*, vol. 11, p. e72435, aug 2022.

[32] D. O. Hebb, *The organization of behavior; a neuropsychological theory.* Wiley, 1949.

[33] S. Song, K. D. Miller, and L. F. Abbott, "Competitive Hebbian learning through spike-timing-dependent synaptic plasticity," *Nature Neuroscience*, vol. 3, no. 9, pp. 919–926, 2000.

[34] T. P. Vogels, H. Sprekeler, F. Zenke, C. Clopath, and W. Gerstner, "Inhibitory plasticity balances excitation and inhibition in sensory pathways and memory networks," *Science*, vol. 334, no. 6062, pp. 1569–1573, 2011.

[35] N. Ravid Tannenbaum and Y. Burak, "Shaping Neural Circuits by High Order Synaptic Interactions," *PLoS Computational Biology*, vol. 12, no. 8, pp. 1–27, 2016.

[36] F. Zenke, E. J. Agnes, and W. Gerstner, "Diverse synaptic plasticity mechanisms orchestrated to form and retrieve memories in spiking neural networks," *Nature Communications*, vol. 6, Apr. 2015.

[37] A. Litwin-Kumar and B. Doiron, "Formation and maintenance of neuronal assemblies through synaptic plasticity," *Nature Communications*, vol. 5, no. May, 2014.

[38] G. Q. Bi and M. M. Poo, "Synaptic modifications in cultured hippocampal neurons: Dependence on spike timing, synaptic strength, and postsynaptic cell type," *Journal of Neuroscience*, vol. 18, no. 24, pp. 10464–10472, 1998.

[39] J. Gjorgjieva, C. Clopath, J. Audet, and J. P. Pfister, "A triplet spike-timing-dependent plasticity model generalizes the Bienenstock-Cooper-Munro rule to higher-order spatiotemporal correlations," *Proceedings of the National Academy of Sciences of the United States of America*, vol. 108, no. 48, pp. 19383–19388, 2011.

[40] L. Montangie, C. Miehl, and J. Gjorgjieva, "Autonomous emergence of connectivity assemblies via spike triplet interactions," *PLOS Computational Biology*, vol. 16, pp. 1–44, 05 2020.

[41] D. Miner and J. Triesch, "Plasticity-Driven Self-Organization under Topological Constraints Accounts for Non-random Features of Cortical Synaptic Wiring," *PLoS Computational Biology*, vol. 12, no. 2, pp. 1–21, 2016.

[42] N. Caporale and Y. Dan, "Spike timing–dependent plasticity: A hebbian learning rule," *Annual Review of Neuroscience*, vol. 31, p. 25–46, July 2008.

[43] D. E. Feldman, "The spike-timing dependence of plasticity," *Neuron*, vol. 75, no. 4, pp. 556–571, 2012.

[44] G. Buzsáki, "Neural Syntax: Cell Assemblies, Synapsembles, and Readers," *Neuron*, vol. 68, no. 3, pp. 362–385, 2010.

[45] C. Miehl and J. Gjorgjieva, "Stability and learning in excitatory synapses by nonlinear inhibitory plasticity," *PLOS Computational Biology*, vol. 18, pp. 1–34, 12 2022.

[46] B. Babadi and L. F. Abbott, "Pairwise analysis can account for network structures arising from spike-timing dependent plasticity," *PLOS Computational Biology*, vol. 9, pp. 1–16, 02 2013.

[47] W. Singer, "Chapter 37 neuronal representations, assemblies and temporal coherence," vol. 95 of *Progress in Brain Research*, pp. 461–474, Elsevier, 1993.

[48] A. Maes, M. Barahona, and C. Clopath, “Learning spatiotemporal signals using a recurrent spiking network that discretizes time,” *PLoS Computational Biology*, vol. 16, no. 1, pp. 1–26, 2020.

[49] M. Loidolt, L. Rudelt, and V. Priesemann, “Sequence memory in recurrent neuronal network can develop without structured input,” *bioRxiv*, 2020.

[50] J. L. Riquelme, M. Hemberger, G. Laurent, and J. Gjorgjieva, “Sequential propagation and routing of activity in a cortical network,” *bioRxiv*, p. 2021.12.21.473652, 2021.

[51] R. Brette and W. Gerstner, “Adaptive exponential integrate-and-fire model as an effective description of neuronal activity,” *Journal of Neurophysiology*, vol. 94, no. 5, pp. 3637–3642, 2005.

[52] I. R. Fiete, W. Senn, C. Z. Wang, and R. H. Hahnloser, “Spike-Time-Dependent Plasticity and Heterosynaptic Competition Organize Networks to Produce Long Scale-Free Sequences of Neural Activity,” *Neuron*, vol. 65, no. 4, pp. 563–576, 2010.

[53] G. G. Turrigiano and S. B. Nelson, “Hebb and homeostasis in neuronal plasticity,” *Current Opinion in Neurobiology*, vol. 10, no. 3, pp. 358–364, 2000.

[54] B. Siddoway, H. Hou, and H. Xia, “Molecular mechanisms of homeostatic synaptic downscaling,” *Neuropharmacology*, vol. 78, pp. 38–44, 2014.

[55] N. S. Desai, L. C. Rutherford, and G. G. Turrigiano, “Plasticity in the intrinsic excitability of cortical pyramidal neurons,” *Nature Neuroscience*, vol. 2, no. 6, pp. 515–520, 1999.

[56] W. Zhang and D. J. Linden, “The other side of the engram: Experience-driven changes in neuronal intrinsic excitability,” *Nature Reviews Neuroscience*, vol. 4, no. 11, pp. 885–900, 2003.

[57] S. Song, P. J. Sjöström, M. Reigl, S. Nelson, and D. B. Chklovskii, “Highly nonrandom features of synaptic connectivity in local cortical circuits,” *PLoS Biology*, vol. 3, no. 3, pp. 0507–0519, 2005.

[58] P. Zheng and J. Triesch, “Robust development of synfire chains from multiple plasticity mechanisms,” *Frontiers in Computational Neuroscience*, vol. 8, no. Article 66, pp. 1–10, 2014.

[59] B. Chambers and J. N. MacLean, “Higher-Order Synaptic Interactions Coordinate Dynamics in Recurrent Networks,” *PLoS Computational Biology*, vol. 12, no. 8, pp. 1–23, 2016.

[60] S. Dorkenwald, N. L. Turner, T. Macrina, K. Lee, R. Lu, J. Wu, A. L. Bodor, A. A. Bleckert, D. Brittain, N. Kemnitz, W. M. Silversmith, D. Ih, J. Zung, A. Zlateski, I. Tartavull, S.-C. Yu, S. Popovych, W. Wong, M. Castro, C. S. Jordan, A. M. Wilson, E. Froudarakis, J. Buchanan, M. M. Takeno, R. Torres, G. Mahalingam, F. Collman, C. M. Schneider-Mizell, D. J. Bumbarger, Y. Li, L. Becker, S. Suckow, J. Reimer, A. S. Tolias, N. Macarico da Costa, R. C. Reid, and H. S. Seung, “Binary and analog variation of synapses between cortical pyramidal neurons,” *eLife*, vol. 11, p. e76120, nov 2022.

[61] N. Hiratani, J. nosuke Teramae, and T. Fukai, “Associative memory model with long-tail-distributed Hebbian 1 synaptic connections,” *Frontiers in Computational Neuroscience*, vol. 6, no. Article 102, pp. 1–15, 2012.

[62] F. I. Kleberg and J. Triesch, “Neural oligarchy: How synaptic plasticity breeds neurons with extreme influence,” *bioRxiv*, pp. 1–31, 2018.

[63] F. Effenberger, J. Jost, and A. Levina, "Self-organization in Balanced State Networks by STDP and Homeostatic Plasticity," *PLoS Computational Biology*, vol. 11, no. 9, pp. 1–30, 2015.

[64] M. Bocchio, C. Gouny, D. Angulo-Garcia, T. Toulat, T. Tressard, E. Quiroli, A. Baude, and R. Cossart, "Hippocampal hub neurons maintain distinct connectivity throughout their lifetime," *Nature Communications*, vol. 11, no. 1, 2020.

[65] M. Chini, M. Hnida, J. K. Kostka, Y.-N. Chen, and I. L. Hanganu-Opatz, "Preconfigured architecture of the developing mouse brain," *Cell Reports*, vol. 43, p. 114267, June 2024.

[66] G. Buzsáki and K. Mizuseki, "The log-dynamic brain: How skewed distributions affect network operations," *Nature Reviews Neuroscience*, vol. 15, no. 4, pp. 264–278, 2014.

[67] P. Zheng, C. Dimitrakakis, and J. Triesch, "Network Self-Organization Explains the Statistics and Dynamics of Synaptic Connection Strengths in Cortex," *PLoS Computational Biology*, vol. 9, no. 1, pp. 1–8, 2013.

[68] Y. Ikegaya, T. Sasaki, D. Ishikawa, N. Honma, K. Tao, N. Takahashi, G. Minamisawa, S. Ujita, and N. Matsuki, "Interpyramid spike transmission stabilizes the sparseness of recurrent network activity," *Cerebral Cortex*, vol. 23, no. 2, pp. 293–304, 2013.

[69] J. N. Teramae and T. Fukai, "Computational implications of lognormally distributed synaptic weights," *Proceedings of the IEEE*, vol. 102, no. 4, pp. 500–512, 2014.

[70] L. N. Driscoll, N. L. Pettit, M. Minderer, S. N. Chettih, and C. D. Harvey, "Dynamic Reorganization of Neuronal Activity Patterns in Parietal Cortex.," *Cell*, vol. 170, no. 5, pp. 986–999.e16, 2017.

[71] E. A. Mankin, G. W. Diehl, F. T. Sparks, S. Leutgeb, and J. K. Leutgeb, "Hippocampal ca2 activity patterns change over time to a larger extent than between spatial contexts," *Neuron*, vol. 85, p. 190–201, Jan. 2015.

[72] K. A. Bolding and K. M. Franks, "Recurrent cortical circuits implement concentration-invariant odor coding," *Science*, vol. 361, Sept. 2018.

[73] G. C. Turner, M. Bazhenov, and G. Laurent, "Olfactory representations bydrosophilamushroom body neurons," *Journal of Neurophysiology*, vol. 99, p. 734–746, Feb. 2008.

[74] Z. S. Zheng, R. Huszár, T. Hainmueller, M. Bartos, A. Williams, and G. Buzsáki, "Perpetual step-like restructuring of hippocampal circuit dynamics," *bioRxiv*, 2024.

[75] K. Yaroslav Felipe Kalle, S. Goedeke, C. Klos, and R.-m. Memmesheimer, "Drifting assemblies for persistent memory : Neuron transitions and unsupervised compensation," *Proceedings of the National Academy of Sciences of the United States of America*, vol. 118, no. 46, p. e2023832118, 2021.

[76] M. E. Rule, A. R. Loback, D. V. Raman, L. N. Driscoll, C. D. Harvey, and T. O'leary, "Stable task information from an unstable neural population," *eLife*, vol. 9, pp. 1–16, 2020.

[77] S. Shoham, D. H. O'Connor, and R. Segev, "How silent is the brain: is there a "dark matter" problem in neuroscience?," *Journal of Comparative Physiology A*, vol. 192, p. 777–784, Mar. 2006.

[78] R. M. French, “Catastrophic forgetting in connectionist networks,” *Trends in Cognitive Sciences*, vol. 3, no. 4, pp. 128–135, 1999.

[79] A. Ecker, B. Bagi, E. Vértes, O. Steinbach-Németh, M. R. Karlócai, O. I. Papp, I. Miklós, N. Hájos, T. F. Freund, A. I. Gulyás, and S. Káli, “Hippocampal sharp wave-ripples and the associated sequence replay emerge from structured synaptic interactions in a network model of area ca3,” *eLife*, vol. 11, p. e71850, jan 2022.

[80] M. Butz and A. van Ooyen, “A Simple Rule for Dendritic Spine and Axonal Bouton Formation Can Account for Cortical Reorganization after Focal Retinal Lesions,” *PLoS Computational Biology*, vol. 9, no. 10, pp. 39–43, 2013.

Supplementary Figures

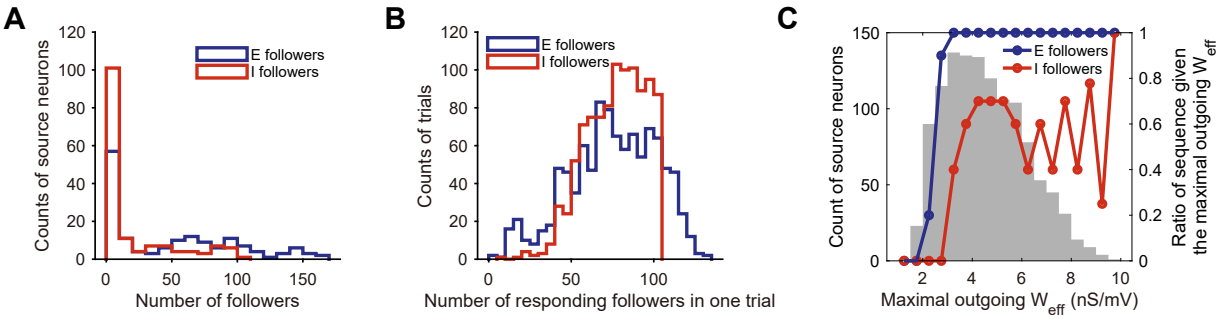

Figure S1. Statistics of sequence generation. A. Distribution of the number of excitatory followers and inhibitory followers of the $n = 155$ source neurons that we tested. **B.** Distribution of the number of followers that spiked after the forced spike of the source neuron. Pooled from 1,000 consecutive trials. **C.** Sequence generation plotted against source neurons' maximal outgoing effective weight. (Gray bars) Histogram of the maximal outgoing W_{eff} of 1,200 neurons in a model network. (Blue line) The ratio of source neurons that had at least one excitatory follower, given the maximal outgoing W_{eff}, calculated within the $n = 155$ source neurons that we chose. (Red line) The ratio of source neurons that had at least one inhibitory follower, given the maximal outgoing W_{eff}, calculated within the $n = 155$ source neurons that we chose.

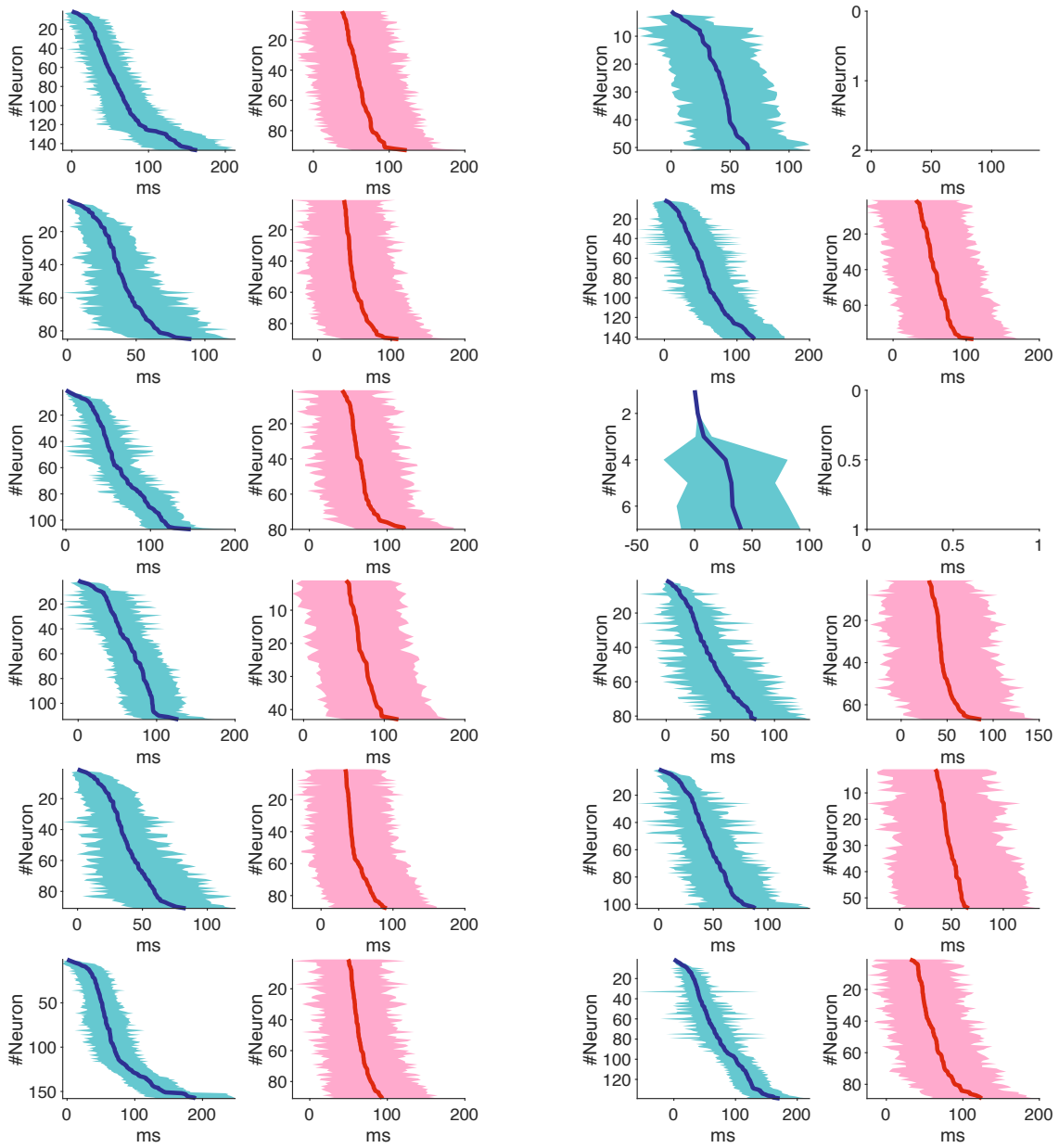

Figure S2. More examples of sequences generated in the same network as in Fig. 1. Blue curves indicate median delays of excitatory followers. Red curves indicate median delays of inhibitory followers. Cyan and pink shades indicate jitters.

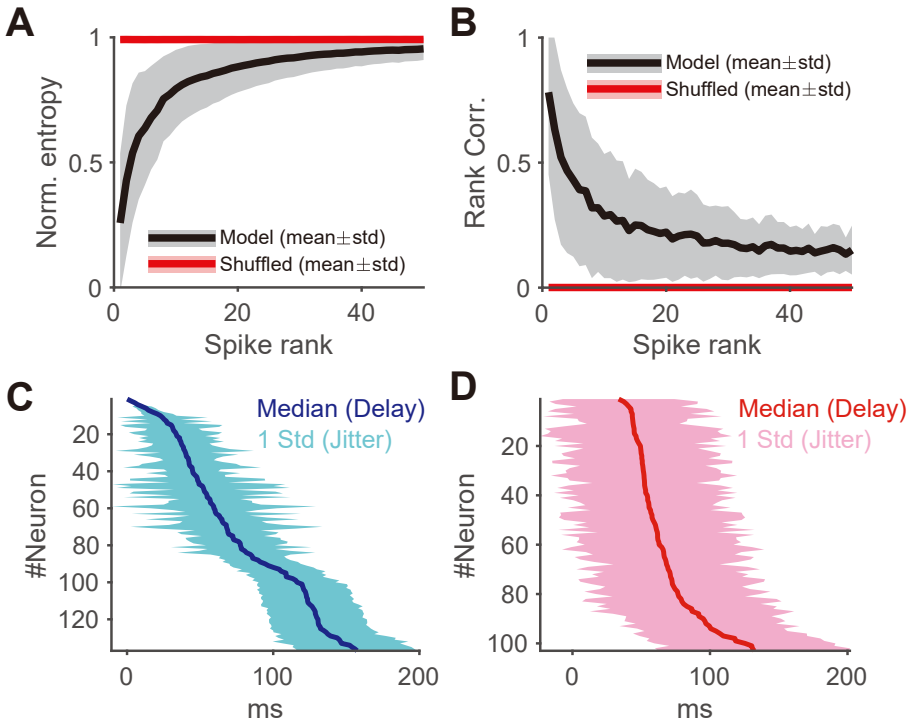

Figure S3. Sequence properties. A. Normalized entropy of sequence in the model network (black) and the null model with shuffled sequences (red). Data pooled from all source neurons with at least one follower ($n = 135$). Each sequence was shuffled 10 times. **B.** Rank correlation as a function of spike rank in the model network (black) and the null model with shuffled sequences (red). Same data as D. **C.** Delay of excitatory followers after source spike. Solid line indicates the median delay and shading indicates the jitter (standard deviation across all trials). **D.** Same as C but for inhibitory followers.

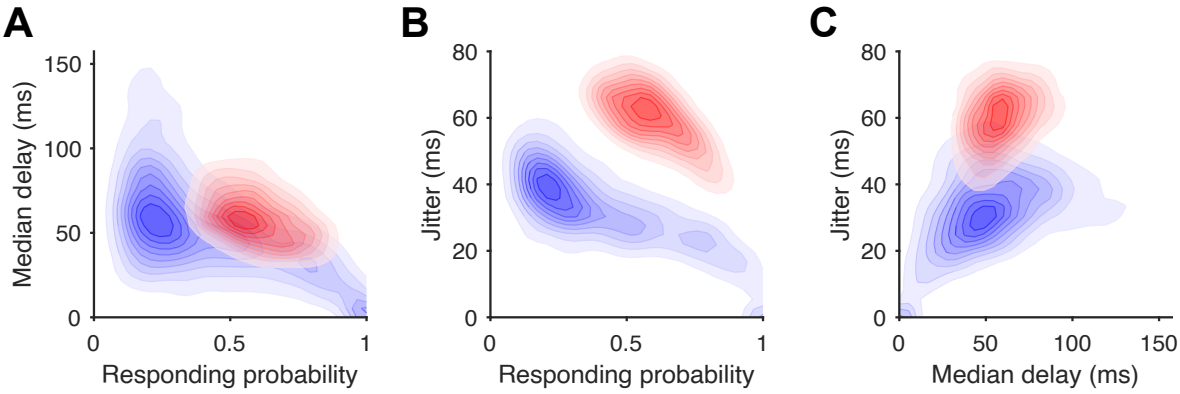

Figure S4. Two dimensional density plot of followers' responding probability, median delay, and jitter. A. Density plot of responding probability and median delay of followers. Median delay is negatively correlated to responding probability. Pearson correlation $r = -0.507$. **B.** Density plot of responding probability and jitter of followers. Jitter is negatively correlated to responding probability. Pearson correlation $r = -0.246$. **C.** Density plot of median delay and jitter of followers. Jitter is positively correlated to median delay. (Blue) Excitatory followers; (Red) Inhibitory followers. Darker color indicates higher probability density. Pearson correlation $r = 0.343$. Pooled over 7,769 excitatory followers and 2,796 inhibitory followers from 135 sequences.

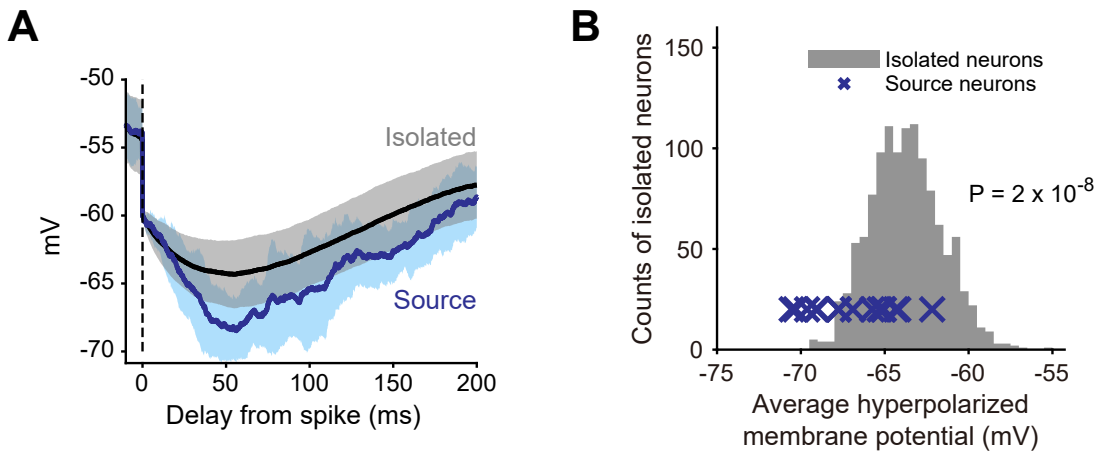

Figure S5. Feedback inhibition from inhibitory followers. A. Source neuron triggers feedback inhibition in the model. Blue: source neuron membrane potential after a spike. Pooled over $n = 15$ neurons. Black: membrane potential of isolated neurons. Pooled over $n = 1,200$ neurons. Solid lines indicate means and shadings the standard deviations. **B.** Quantification of feedback inhibition (A). The average hyperpolarized membrane potential is quantified as the mean of the membrane potential within 50 ms to 100 ms after the spike.

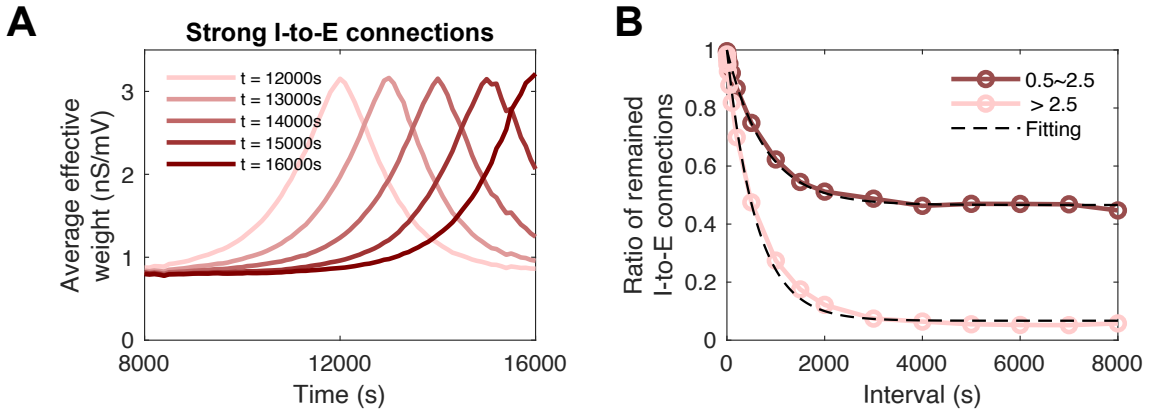

Figure S6. The turnover of I-to-E connections. A. Average strength of multiple groups of I-to-E connections picked from the tail of the W_{eff} distribution at different time points, after the weight distribution has reached a steady state. **B.** The decay rate of strong I-to-E weights ($W_{\text{eff}} > 2.5$) and weak I-to-E connections ($0.5 < W_{\text{eff}} < 2.5$). Dots indicate ratios calculated from simulations with 10 instantiations of the network. Dashed lines indicate exponential fits with different time constants and baselines for each group.

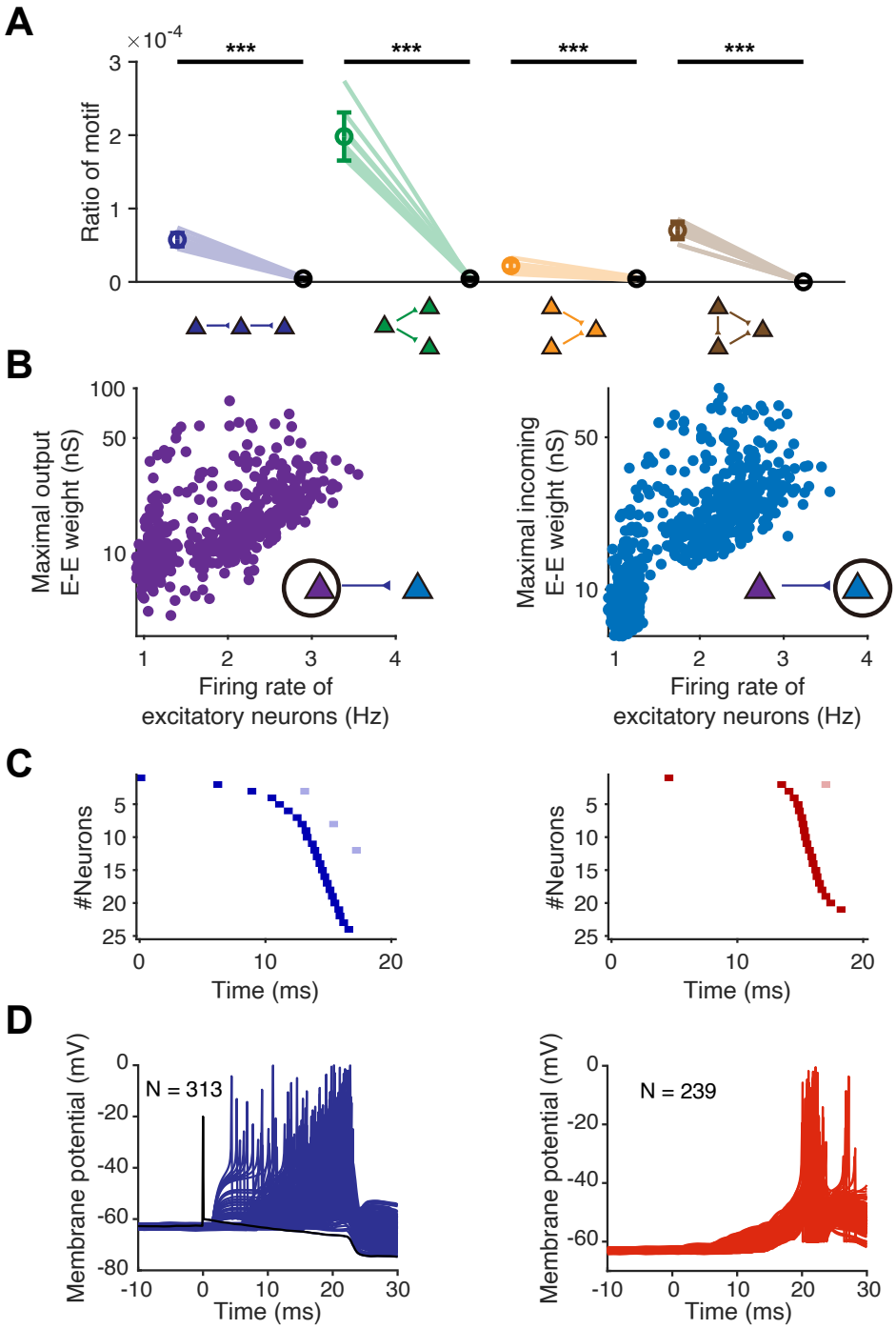

Figure S7. A model network without presynaptic normalization and intrinsic plasticity generates hub neurons and short sequences. A. The comparison between the ratio of motifs at $t = 6,000$ s in the alternative model network with hub neurons and the estimated ratio in a random control network given the p_0 value at that time point. Calculated from 10 trials. Error bars represent standard deviation. ***: $P < 0.001$. **B.** Hub neurons. The synaptic strength is proportional to the firing rate of neurons. Neurons with a high firing rate have a much greater impact on the network dynamics. Left: presynaptic neurons in E-to-E connections. Right: Postsynaptic neurons in E-to-E connections. **C.** Short sequences as a result of hub neurons. Left: excitatory followers. Right: inhibitory followers. **D.** Explosive dynamics in which a great number of followers can be generated within a time window as short as 30 ms. Left: excitatory neurons. Right: inhibitory neurons.

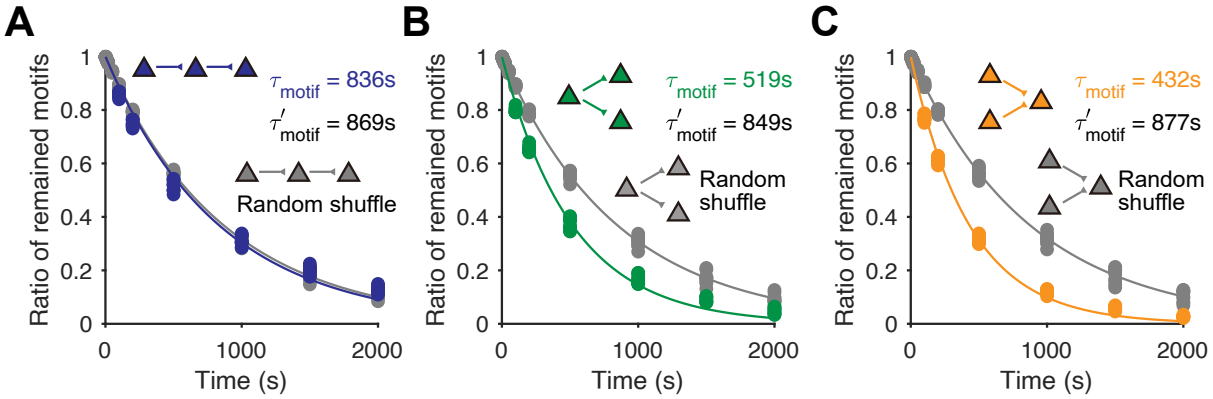

Figure S8. The decay of three-neuron motifs in our model network (color-coded) and in the null model (gray) in which the connections were shuffled. A. Linear chains. The decay of linear chains in our model network was comparable to the null model, consistent with Fig. 3D in which the ratio of linear chains was comparable to the null model. **B.** divergence motifs. The decay of divergence motifs in our model network was much faster than the null model, consistent with Fig. 3D in which the ratio of divergence motif was much lower than the null model. **C.** Convergence motifs. The decay of convergence motifs in our model network was much faster than the null model, consistent with Fig. 3D in which the ratio of convergence motifs was much lower than the null model.

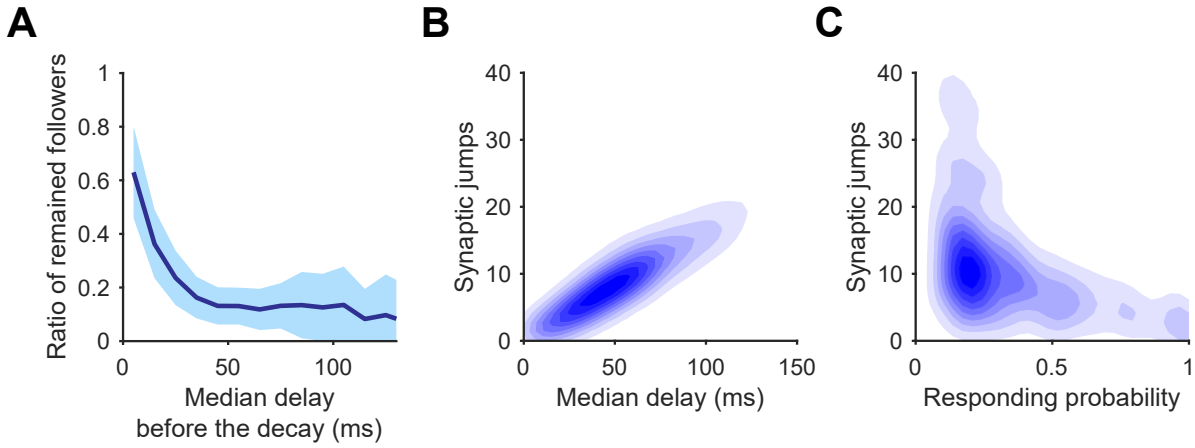

Figure S9. A. The remained ratio of followers after a 1,000 s interval decreases with the median delay of followers. Solid line indicates the average and shade represents the standard deviation. **B.** The strong synaptic jump is negatively correlated to the responding probability. Pearson's correlation $r = -0.386$, pooled over 2,508 followers at $t = 8,000$ s in Fig. 4. **C.** The strong synaptic jump is positively correlated to the median delay. Pearson's correlation $r = 0.494$, same followers as B.

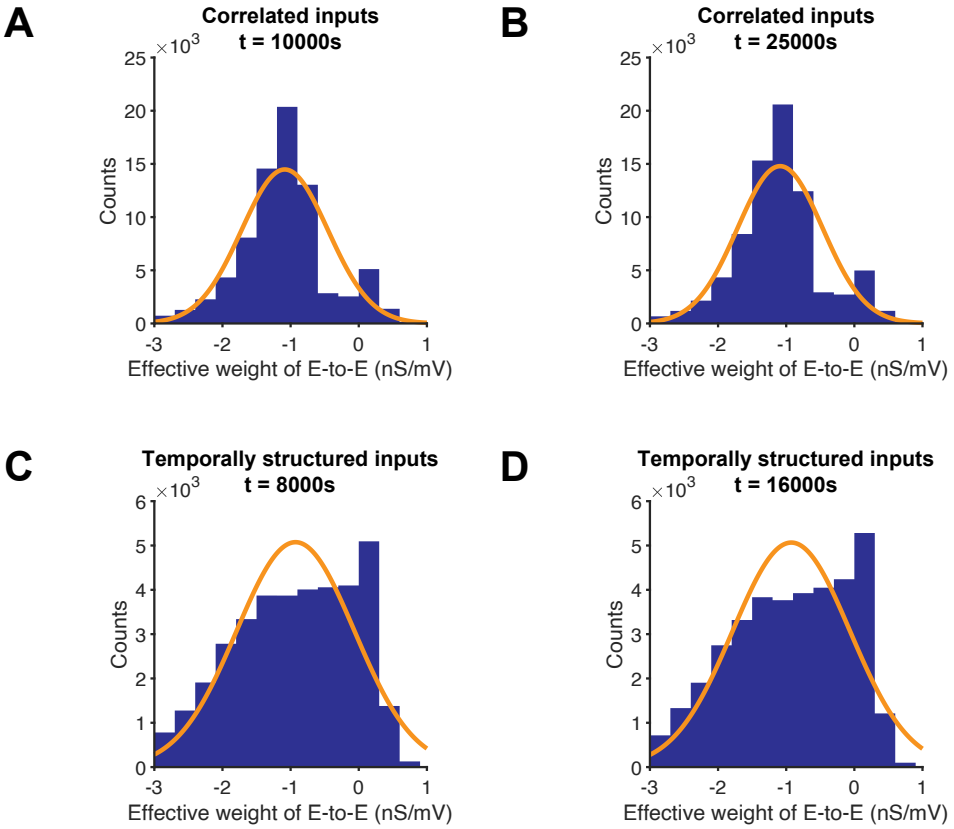

Figure S10. E-to-E distribution reached a steady state after training with structured inputs. A. The network develops a stable distribution which can be fit as lognormal when trained with correlated inputs. Left: $t = 10,000$ s, right: $t = 25,000$ s, orange curve shows the fit, $R^2 = 0.809$ for the left and $R^2 = 0.821$ for the right. **B.** The network develops a stable distribution which can be fit as lognormal when trained with temporally structured inputs. Left: $t = 8,000$ s, right: $t = 16,000$ s, orange curve shows the fit, $R^2 = 0.669$ for the left and $R^2 = 0.669$ for the right.